Climate change and topography as drivers of Latin American biome dynamics

Flantua, S.G.A.

Publication date
2017
Document Version
Other version
License
Other

Geological and climatic determinants of mountain biodiversity

CHAPTER 8

THESIS OUTLINE

A. LOCATION ANALYSIS

Chapter 2
Updated site compilation of the Latin American Pollen Database

B. CONDITION ANALYSIS

Chapter 3
Geochronological database and classification system for age uncertainties in Neotropical pollen records

C. TRENDS ANALYSIS

Chapter 4
Climate variability and human impact in South America during the last 2000 years: synthesis and perspectives from pollen records

Chapter 5
Application of GIS and logistic regression to fossil pollen data in modelling present and past spatial distribution of the Colombian savanna

D. PATTERN ANALYSIS

Chapter 6
Connectivity dynamics since the Last Glacial Maximum in the northern Andes; a pollen-driven framework to assess potential migration

Chapter 8
Geological and climatic determinants of mountain biodiversity

Chapter 7
Historical connectivity and mountain biodiversity

Chapter 9
Unravelling the mountain fingerprint: topography, paleoclimate and connectivity as drivers of contemporary biodiversity patterns in the Northern Andes

PREFACE

This chapter is currently under revision after first submission (with invitation to resubmit) in Nature Geoscience as:
Antonelli, A., Kissling, D., **Flantua, S.G.A.**, Bermúdez, M.A., Mulch, A., Muellner-Riehl, A.N., Kreft, H., Linder, H.P., Badgley, C., Fjeldså, J., Fritz, S.A., Rahbek, C., Herman, F., Hooghiemstra, H., Hoorn, C. Geological and climatic determinants of mountain biodiversity.

This chapter consists of an overview paper that addresses mountain biodiversity on a global scale. The relationship between geology and biodiversity is explored with state-of-the-art datasets that provide an insight into long-term landscape evolution driving mountainous hotspots of biodiversity. The reason this chapter suits this thesis is the complementary value of understanding the paleohistory of mountains on very different spatial and temporal scales than addressed in the previous chapters. Chapter 7 focuses primarily on drivers of Andean biodiversity on a relatively short time scale in geological terms, while this chapter puts previous work into the perspective through reviewing the importance of long-term geological processes.

To explain contemporary mountain biodiversity, the effects of geological and environmental variables are quantified. In terms of geology, the relative importance on species richness is evaluated by using the timing of exhumation, erosion rates, topography and soils. What becomes evident, and not unsurprisingly, is that climate displays itself as an important explanatory variable for every mountain system around the world. Numerous papers have confirmed the high correlation between contemporary species richness and environment. However, the high correlation does not necessarily explain the main processes driving species richness. Here, the geological history is bound to play an important role. The observed diversity-geology relationship shows a more diverse responsiveness in different mountain systems around the world. In some cases long term erosion is a strong predictor of mountain diversity, while in other recent erosion and climate conditions seem to overrule historically deep time processes. The overview provided in this chapter shows the spatial and temporal complexity of mountain building throughout the globe and hints at the geological variables influencing the buildup of species richness.

Article submission to *Nature Geoscience (Revision of NGS-2015-11-02271)*
Manuscript type: *Review article*

Title: **Geological and climatic determinants of mountain biodiversity**

Authors and affiliations: Alexandre Antonelli[1,2,3*§], W. Daniel Kissling[4§], Suzette G.A. Flantua[4§], Mauricio A. Bermúdez[5§], Andreas Mulch[6], Alexandra N. Muellner-Riehl[7,8], Holger Kreft[9], H. Peter Linder[10], Catherine Badgley[11], Jon Fjeldså[12], Susanne A. Fritz[6], Carsten Rahbek[12,13], Frédéric Herman[14], Henry Hooghiemstra[3], and Carina Hoorn[4,*§]

[1]Department of Biological and Environmental Sciences, University of Gothenburg, Box 461, SE 405 30 Göteborg, Sweden
[2]Gothenburg Botanical Garden, SE-41319 Göteborg, Sweden
[3]Gothenburg Global Biodiversity Centre, Box 461, SE-405 30 Göteborg, Sweden
[4]Institute for Biodiversity and Ecosystem Dynamics, University of Amsterdam, P.O. Box 94248, 1090 GE Amsterdam, The Netherlands
[5]Facultad de Ciencias Naturales y Matemáticas, Universidad de Ibagué, Colombia
[6]Senckenberg Gesellschaft für Naturforschung, Biodiversität und Klima Forschungszentrum, 60325 Frankfurt/Main, Germany
[7]Department of Molecular Evolution and Plant Systematics & Herbarium (LZ), Institute of Biology, Leipzig University, D-04103 Leipzig, Germany
[8]German Centre for Integrative Biodiversity Research (iDiv) Halle-Jena-Leipzig, D-04103 Leipzig, Germany
[9]Biodiversity, Macroecology & Conservation Biogeography, Georg-August-University of Göttingen, 37077 Göttingen, Germany
[10]Department of Systematic and Evolutionary Botany, University of Zurich, CH-8008 Zurich, Switzerland
[11]University of Michigan, Department of Ecology & Evolutionary Biology, Ann Arbor, USA
[12]Center for Macroecology, Evolution and Climate, Natural History Museum of Denmark, University of Copenhagen, Denmark.
[13]Department of Life Sciences, Imperial College London, Silwood Park campus, Ascot SL5 7PY, U.K.
[14]Institute of Earth Surface Dynamics, University of Lausanne, Lausanne, Switzerland

[*]Authors for correspondence: Alexandre Antonelli (alexandre.antonelli@bioenv.gu.se), Carina Hoorn (M.C.Hoorn@uva.nl)

[§]These authors contributed equally to this work.

Preface

Mountains are key features of the Earth's surface and contain a substantial proportion of the world's species. However, the links between the evolution and distribution of species and the formation of mountains remain poorly understood. Here, we assess the relationship among species richness, geology and climate by integrating existing databases and analysing erosion, relief, soil, climate, and their relation to the geographical distribution of terrestrial vertebrates at global and regional scales. Sites with the greatest species richness correlate with those areas that have the highest annual rainfall and temperatures. Moreover, a link between mountain building processes and

biodiversity is also observed, with species richness correlating with topographic relief, erosion rates on geological timescales, cooling age and heterogeneity of soil types. This link is prominent but under-explored, and likely relates to the feedbacks between uplift and atmospheric circulation through time, mountain orientation and location, and their impact on species diversification and biotic migrations. A better understanding of biosphere-lithosphere interactions would contribute to predicting mountain biodiversity across space and time.

Lithosphere dynamics, including rock formation, exhumation, surface uplift and relief development, as well as related climate change and variability, create diverse environments in mountainous regions (Box 1). Mountain building establishes topographic complexity and creates new habitats where species evolve and diversify[1,2,3]. It also provides nutrients to surrounding lowlands, increases sediment delivery and heterogeneity of soil types, affects local and regional climates, facilitates the establishment of immigrant species, leads to *in situ* speciation, and provides neighbouring areas with newly formed species [4,5, 6,7,8,9]. At the same time, biome changes linked to orogeny [10,11,12], such as formation of special montane forest types, grassland or alpine vegetation, feed back into climatic and tectonic processes [13, 14]. Biological and geological processes are therefore closely linked, although causal mechanisms frequently remain elusive.

Recent advances in the study of Earth's surface processes include stable isotope palaeoaltimetry[15,16,6] and continued growth of thermochronometric techniques that can be used to constrain the rate and timing of mountain erosion[17]. These advances parallel new methods and increasingly large public databases that allow the estimation of how and where species are distributed (e.g. [18]) and when and under which conditions they originated and diversified[19,20,21]. Macroevolutionary, genetic and stable isotopic methods, coupled with growing datasets on species distributions, bedrock age, soil types, palaeoaltimetry, and climate, constitute an unprecedented opportunity to explore how geological and evolutionary processes have interacted in Earth history[22, 23].

Present-day global and regional biodiversity (Box 2) is highly correlated with contemporary climate, especially temperature and precipitation, meaning that warm and wet climates generally sustain the highest species richness[24,25]. Biodiversity is also greater in heterogeneous environments, e.g., comprising many soil types and varied topography[26,27,28,29]. Correlative analysis of present-day climate and environmental heterogeneity can explain 50–70% of the variation in regional and global plant and animal species richness[25,30]. Furthermore, strong correlations between climate and biodiversity are not only evident today [31,32,33] but have probably existed for millions of years[34,35,36,37,38]. However, many important geological processes and variables have not yet been comprehensively assessed when analysing global and regional biodiversity.

Quantifying long-term processes that underlie biodiversity patterns and dynamics is challenging. Such processes include species diversification and dispersal, long-term landscape evolution, and geological and climatic history [39,40,2,33,22]. In addition, observed diversity-environment relationships are often scale dependent (Box 2), and are stronger for species with large geographic ranges than for small-ranged species whose distributions are more strongly linked to topographic complexity than climatic factors[41,42]. Such narrowly distributed species are the main feature of the outstanding diversity of mountain regions, strengthening the case for a role of mountain building in generating high biodiversity[43,2].

Here, we explore links and feedbacks among mountain biodiversity, geology, and climate. Many of the world's centres of animal and plant biodiversity coincide with mountain systems, which show contrasting orientations and continental positions (Fig. 1a). We evaluate this apparent correlation with several previously generated geological, climatic and biological datasets, and quantify the relative importance of climate, cooling age (the onset of exhumation of rocks, or in other words their transport to the Earth's surface, as measured by apatite fission-track ages), erosion rates, topography, and soil heterogeneity on species richness. We focus our analyses on terrestrial vertebrates (including birds, mammals and amphibians), whose global species distributions are comparatively well known (Fig. 1b), in contrast to those of plants, fungi, invertebrates and other organisms. We find that relief, cooling age, erosion rates and soil heterogeneity are strong predictors of mountain biodiversity and conclude that geological processes are essential for understanding the evolution and distribution of biodiversity at global and regional scales.

Global determinants of mountain biodiversity

We compiled a global dataset at 1° resolution reflecting the distribution of terrestrial vertebrate diversity (Fig. 1b) as well as nine predictor variables (Table 1). These variables were related to climate (precipitation, temperature and their seasonality) and geology (topographic relief, cooling age, long- and short-term erosion rates, and heterogeneity of soil types; see Methods and Supplementary Information) and used as predictors in statistical models to explain spatial variation in vertebrate species richness (the response variable) within and across mountain regions worldwide. We included grid cells that contained the required geological information and lay predominantly above 500 m, thereby excluding lowland areas (see Methods). We used multiple regression models to explain spatial variation in vertebrate species richness as a function of the 9 predictor variables. Of the 20,866 species for which distribution data were available, nearly half (10,340) occur in our mountain dataset.

For climatic variables, the global analysis shows that annual precipitation and mean annual temperature are the two most important predictors of mountain biodiversity, although there is substantial variation among individual sites (Fig. 2a). Both precipitation and temperature exert a positive effect, i.e., most mountain species are found in places with high rainfall and warm temperatures (Fig. 2b,c). The relationship with species richness is linear for temperature and non-linear for precipitation, i.e., the number of species levels off above a threshold of c. 1500 mm rainfall per year (Fig. 2b). These results substantiate previous studies and suggest that water availability and temperature are key factors for predicting latitudinal and elevational gradients of biodiversity for terrestrial vertebrates[25,44,45,46].

Beyond climate, our analyses provide a first quantitative assessment of the relative importance of geological factors in explaining variation in species richness across the world's mountains. Topographic relief, cooling age, short-term erosion rate and heterogeneity of soil types are statistically significant predictors in the global model (Fig. 2a). The relationships with relief, short-term erosion and soil types (Fig. 2d,f,g) are positive and linear, probably reflecting a higher carrying capacity of biodiversity in environmentally heterogeneous habitats[29]. In addition, high diversity in mountain regions is accentuated by the overlap of widespread species, and high turnover of species with narrow distributions[41]. These relationships expand our understanding of how environmental heterogeneity and species richness are related and suggest a key role of geological processes in shaping global biodiversity.

Regional assessments

Around the world, mountain ranges have different geological histories, spatial configurations, and orientation in relation to atmospheric circulation patterns, and show different biodiversity patterns (see Fig. 3a and Supplementary Information for characterisation of all mountain systems surveyed here). These characteristics influence temperature gradients, orographic precipitation, seasonality, runoff and associated sediment evacuation[47,48,49]. In addition, mountains form in different biogeographic settings, with different levels of pre-existing biodiversity and regional species pools surrounding them[50]. Hence, species may respond differently to the abiotic environment in different regions and determinants of species richness at the global scale may therefore not reflect those at regional scales. We explored this possibility through separate analyses of mountain regions for which statistically sufficient data were available (Fig. 3b–e): North America, the Andes, Eastern Africa, and High Asia.

In all regional models (Fig. 3b–e), climate remains the strongest correlate of species richness, but with varying importance of each variable (precipitation, temperature, and their seasonality) and sometimes contrasting directions of effect (positive or negative). Geological variables are important predictors in all regions, but with varying strength and direction of effect. Below we discuss the likely factors underlying the distinctive results for each region.

North America

Current mountain vertebrate richness (Fig. 3b, Supplementary Fig. S1) peaks in the northern Rocky Mountains, the western edge of the Colorado Plateau, and the southern Sierra Nevada of California. The positive relationship between annual precipitation and richness peaks at c. 600–800 mm/year (Fig. S1) and may reflect the opposing trends of high amphibian richness in areas of higher rainfall versus high mammal and bird richness in areas of high precipitation seasonality and lower rainfall[24,51,52]. Temperature range has the strongest effect among the climatic variables (Fig. 3b). The strong positive relationship with diversity contrasts with a negative relationship described for the lowlands[51]. This is likely because annual temperature range is high over the Colorado Rocky Mountains and westward into the Great Basin, where vertebrate richness is also high, and low along the humid Pacific coast, where vertebrate richness is relatively low. Soil heterogeneity is the strongest geological predictor variable, supplemented by long-term erosion and topographic relief (Fig. 3b). Long-term erosion is negatively correlated with species richness, suggesting that areas with strong erosion have low species richness, possibly as a result of glaciations in western North America and highly weathered landscapes.

The Andes

Diversity is highest across the relatively young northern Andes where relief, short-term and long-term erosion are also high (Fig. S2a). High Andean diversity is strongly correlated with high annual rainfall, but temperature gradients and precipitation seasonality also play a role (Fig. 3c, Fig. S2). Among geological variables, topographic relief and short-term erosion play important roles (Fig. 3c). In the relatively young northern Andes, high diversity can be related to mountain uplift[53], which allowed the establishment and subsequent local diversification of cool-adapted lineages of animals[2] and plants[54], although a connection between diversification and orogeny is not always evident[55]. This area is also characterised by many recent species radiations, commonly linked to the influence of glacial-interglacial cycles[56,57]. In the older, central Andes, the orographic barrier is particularly strong, with a warm, wet northeastern side reflecting high diversity (Fig. 3a, red colours), and a colder and drier southwestern side reflecting low diversity (Fig. 3a, blue colours). In the southern Andes,

precipitation patterns are opposite to those in the central and northern Andes. Predominant advection of moisture there comes from the Pacific and creates orographic rainfall in the west (where diversity is highest) and a prominent rain shadow, and less species of both plants and animals in Patagonia in the east.

Eastern Africa

Species richness of terrestrial vertebrates peaks in high rainfall areas and decreases where precipitation seasonality is high (Fig. 3d, Fig. S3). The region is characterised by many endemic species[58], resulting in high overall biodiversity (Fig. 3a). Three geological predictor variables, namely cooling age, long-term erosion rate and soil heterogeneity, show equally strong correlations with vertebrate species richness (Fig. 3d). This region is geologically different to the other regions, shaped by rifting processes, widespread volcanic activity, glaciations, and parallel uplift and subsidence[59]. Relatively young mountain orogeny (rifting during the Miocene and Pliocene[60] resemble the Andes, but here cooling ages are among the highest from our global analysis, reflecting deep-time exhumation history, while long term erosion values are relatively low[61]. Both are negatively correlated with biodiversity (Figs. 3d, S3), suggesting that high cooling age and long term erosion relate to low species richness. Echoing the geological history of young and old mountain formations, biodiversity consists of recent radiations as well as older relict taxa[62].

High Asia

The Central Asian highlands (hereafter 'High Asia') include the Qinghai-Tibetan Plateau and the Tianshan, Hindu-Kush, Himalayan and Hengduanshan mountain regions (Fig. 3a). High Asia harbours a high diversity of vertebrates (Fig. 3a) as well as vascular plants[63]. Vertebrate diversity is highest in the southern and southeastern parts of the region, reflecting a strong positive effect of precipitation and temperature on species richness (Fig. 3e). This region is under pronounced influence of both South Asian and East Asian monsoons, and is dominated by a warm, humid climate and subtropical-tropical vegetation[64], which co-occurs with high biodiversity (Fig. 3a). In contrast, the temperature extremes on the Qinghai-Tibetan Plateau, which are reflected in high temperature seasonality, coincide with low species diversity and explain the negative relationship between vertebrate diversity and temperature annual range (Fig. 3e). Among geological variables, which similarly to climatic variables show large regional variations (Fig. S5, Fig. S6), cooling age and long-term erosion are the strongest predictors of vertebrate diversity (Fig. 3e). The highest erosion rates (long and short term) are found where climate and topographic gradients are strongest (Himalayan and Hengduanshan mountain regions), reflecting the strong climate-topography interaction over different time scales. Cooling ages show a similar positive effect on species richness, indicating that vertebrate diversity peaks in areas where environmental heterogeneity is high. Biodiversity in this region stems from deep-time speciation due to mountain uplift and related climate changes[8] and recent diversification related to Quaternary climate oscillations[65].

From patterns to processes

Our global and regional assessment of geological and climatic variables and their relation with biodiversity highlights that i) precipitation and temperature are the most important predictors; and ii) topographic relief, cooling age, erosion rates and soils also play an important role. We note that all studied mountain ranges in the Inter-Tropical Convergence Zone are perpendicular in orientation relative to atmospheric circulation, and hence strongly alter regional and global climate. Moreover, all mountain ranges have areas with high precipitation (Fig. S5), reflecting orographic rainfall when moist air is forced upwards over

mountain terrain. Ultimately it is mountain building that drives regional climate, and thus the high precipitation patterns and temperatures that shape biodiversity.

In contrast to climate, cooling ages and erosion rates vary depending on the orogenic history of the mountains (Fig. S6a–e). For instance, cooling ages are highest in Eastern South America, Africa and Australia (Fig. S6b) whereas high erosion (following climatic fluctuations) is particularly evident in the northern and southern Andes, southern High Asia and the European Alps (Fig. S6c–d). This partly reflects that convergence and uplift have been significant in the last 10 Myr and that convergence is still ongoing, but less so in areas with older tectonic activity. This may explain why long-term erosion has opposite effects on species richness in Eastern Africa and High Asia (Fig. 3), and why erosion and cooling ages show different trends in the global and regional analyses Fig. 2, Fig. 3).

To fully understand the patterns and correlative relationships identified here, we also need to understand the underlying ecological and evolutionary processes on long and short time scales, involving both biotic and abiotic factors[66,67]. Our results suggest a strong interaction between mountains and biodiversity, which could take form in various ways and at different stages (Fig. 4). For instance, terrain uplift occurs through tectonism, volcanism and isostasy over millions of years. This process has affected regional climates through orographic precipitation and elevational temperature gradients (Fig. 4a), and even global climates through effects on global circulation patterns. As a consequence, vegetation changes along elevational gradients[9], and this creates ecological opportunities for species to adapt to different vegetation zones. Nevertheless, how biodiversity changes along these elevational gradients varies across mountains[46] and species richness gradients might peak at different elevations.

Biodiversity in any system —whether a mountain, island or continent— is ultimately regulated by three processes: speciation, extinction, and dispersal[68]. Mountains may increase speciation by causing genetic isolation of once connected populations, leading to an increase in species richness (Fig. 4d). This is facilitated by the creation of novel habitats and niche spaces that may be quickly filled by species radiations[69, 70], resulting in many endemic species adapted to particular climate regimes, soil types and vegetation belts[9]. Climatic fluctuations of the Plio-Pleistocene have also led to drastic changes in mountains at temperate and tropical latitudes. In high mountains (at latitudes and altitudes prone to repetitive glaciations), surface processes strongly reshaped the relief through denudation and erosion. This has increased environmental heterogeneity and created diverse microclimates, further favouring speciation.

Species may also go extinct (Fig. 4e) as tectonic activity ceases, mountains decay and habitats disappear due to erosion, similarly to what happens when volcanic islands and their biota subside[68]. Furthermore, entire populations can be annihilated by stochastic events such as landslides and eruptions, or if high-elevation species have nowhere to go when global warming drives them upslope[71]. Mountain biodiversity can also increase with the arrival of immigrant species from other mountain systems (Fig. 4f), either through active or passive dispersal (e.g., flying birds or bats and the seeds they carry). Climatic fluctuations can then trigger dispersal of populations between peaks and valleys, leading to further opportunities for speciation by isolation and secondary contacts. Mountains may also sustain ancient organisms that only need to move short distances to keep their preferred environment during climate change[72]. Mountains thus constitute dynamic systems and act as cradles and museums of biodiversity.

Looking ahead

To further advance the integration of geological and biological sciences, we do not only need more data: we also need to carry out new analyses of both biotic and abiotic parameters. From biology, increased and higher resolution data on current and past species distributions and diversity patterns are extremely important, focusing on poorly explored areas and less-studied taxonomic groups, such as invertebrates along elevational gradients in tropical mountains[73]. It is furthermore important to understand species' characteristics (i.e., ecological traits and biotic interactions) because these influence species coexistence[74], affect responses of species to environmental gradients and determine their functional role in ecosystems[75]. Beyond taxonomic and functional analyses, we also need to analyse phylogenetic diversity and the evolutionary history of organisms[76].

Opportunities for the Earth sciences are equally manifold. We highlight the need for interfacing Earth surface-processes and tectonic studies with phylogenetic techniques to facilitate comparisons of competing hypotheses with respect to the timing of surface uplift[77, 78,3]. Similarly, compilations of biologically relevant variables identified here in both past and present environments would provide essential insights currently insufficiently integrated. Finally, we need to establish robust palaeoaltimetry reconstructions and accurate erosion-rate histories that take into account topographically induced feedbacks in the global climate system, including changes in atmospheric circulation.

We thus urge geoscientists to enhance their efforts in understanding feedbacks between topography, erosion and atmospheric circulation through time, and biologists to include Earth surface processes and palaeoaltimetry data into biodiversity models. Integrating approaches and data from biology and geosciences into a common research framework is still in its infancy, but undoubtedly opens new research avenues for understanding the distribution and evolution of life on Earth.

ACKNOWLEDGMENTS

We thank A. Rohrmann, R. Moucha, V. Mosbrugger, F. Condamine and C. Bacon for early discussions and support, and three anonymous reviewers and the Editor for substantial advice. Funding for this work was provided by the Swedish Research Council (B0569601), the European Research Council under the European Union's Seventh Framework Programme (FP/2007-2013, ERC Grant Agreement n. 331024), the Swedish Foundation for Strategic Research and a Wallenberg Academy Fellowship to A.A.; a German Science Foundation DFG grant Mu2845/4-1 and an A. Cox Fellowship (Stanford University) to A.M.; a University of Amsterdam starting grant to W.D.K.; a Netherlands Organization for Scientific Research (NWO) grant (2012/13248/ALW) to S.G.A.F; a German Science Foundation DFG grant (FR 3246/2-1) to S.A.F; a German Science Foundation DFG grant (MU 2934/2-1) to A.N.M.-R.; and the sFossil workshop at the Synthesis Centre for Biodiversity Sciences sDiv (DFG grant FZT 118).

AUTHOR CONTRIBUTIONS

C.H., A.A. and A.M. initiated the project; A.A., C.H., W.D.K. and S.G.A.F. coordinated the work and led the writing with contributions from all authors; C.R. provided access to the bird data; S.G.A.F, M.A.B and S.A.F. compiled, cleaned and standardised all data; W.D.K. performed the analyses.

BOX 1 | Mountain building, climate, and erosion

Global topography reflects the interplay of geodynamic and climatic processes that shape the Earth's surface. It is intimately linked to biodiversity in mountain systems through a multitude of gradients (e.g. temperature, relief, rainfall, weathering) and through the geographical orientation of mountains in relation to atmospheric circulation patterns.

One of the key questions among biogeographers and ecologists is: *What influence do mountain building and climate have on the evolution and distribution of species, and how can these factors be teased apart* [3, 25]? This debate parallels a paradigm shift that has unfolded in the geoscience community. For three decades, geoscientists have been wondering: *Are the highest peaks in the world formed only due to tectonic processes, or does the sedimentary record observed around mountain belts in the world involve a positive feedback between climate change and tectonics as a consequence of Plio-Pleistocene climatic oscillations*[82]*?*

As a consequence, reconstructing topography of the world's largest mountain ranges has gained considerable momentum mainly through the advent of stable isotope palaeoaltimetry (e.g.[83,84,85]). Available data indicate that some mountain systems such as the Southern Alps and parts of the central Andes (e.g. [83,86]) have uplifted fast and relatively recently while others show clear evidence for Neogene (European Alps, Himalaya[87, 88]) or even older (e.g. North American Cordillera; Tibet[89,90]) topography.

Mountains are high when the density and thermal structure of the continental crust (and upper mantle) result in high buoyancy (i.e. high upward force exerted by the mantle). Global topography is therefore the combined result of isostasy (i.e. floating of the Earth's crust at an elevation that depends on its thickness and density) with respect to the upper mantle, tectonic processes that modify the density structure of the crust and surface processes such as erosion, sedimentation and anthropogenic land use that shape our planet. Because of the height these mountains achieved, they interfered with global atmospheric circulation patterns and contributed to Plio-Pleistocene global cooling (e.g.[91,92,93]). Intensified erosion may have enhanced weathering of silicate-rich rocks, fostering chemical reactions that promote removal of CO_2 from the atmosphere and storage in the sedimentary record of continental and marine basins. This process exacerbated the intensity of long-term climate change while effectively reshaping mountain relief. Because erosion is not necessarily uniform, with rivers and glaciers incising valley bottoms, isostasy can induce uplift of mountain peaks while overall elevation decreases[82].

Advances in the field of thermochronology now enable geoscientists to accurately quantify timing and rates of erosion and exhumation – and thus estimate relief formation – around the globe[94]. The migration of rock towards the Earth's surface can be measured within minerals that preserve the timing of when thermal boundaries in the upper 10 km of the crust were crossed. This and other recent techniques make it possible to quantify global long-term erosion patterns with a sedimentary record of Neogene-Quaternary age (e.g.[95]. Meta-analyses of global databases on erosion rates through time show a significant increase in erosion since 6 Ma, and especially since 2 Ma. These increases in erosion rates occur at all latitudes, but mostly in glaciated terrains. Slow erosion characterises Australia and Scandinavia, and very high rates —especially at mid-latitudes— are common in the Southern Alps, Taiwan, Papua New Guinea, the Himalayas, the Andes and Alaska[96,17].

Collectively, the interplay of surface uplift, weathering and erosion, relief development and climate change set the stage for biological evolution on local to regional scales.

BOX 2 | Mountain biodiversity

Biological diversity (biodiversity) describes the variation of life at all levels of biological organization[97,98]. Among several available biodiversity measures, the most commonly used is species richness, a simple count of the number of species in an area. While species richness treats all species equally, other biodiversity measures such as (phylo)genetic and functional diversity[99]. We consider the relatedness and the differences in morphological, physiological and phenological traits of species in a community[100]. All patterns of biodiversity strongly depend on the spatial scale at which they are measured, which is particularly important for mountains (Fig. B2).

Biologists often differentiate among alpha-, beta-, and gamma-diversity[101]. Alpha-diversity refers to the species richness measured at small spatial scales (such as plots, transects and mountain tops). Beta-diversity describes the change in species composition over space, e.g., from one plot or one community to the other[102]. Gamma-diversity is the number of species in a larger spatial unit, e.g., in an entire mountain range or a grid cell (as used in this study).

Different data sources can be used to study patterns of mountain biodiversity: (i) Range maps, which are polygons that depict the distribution of a species, usually drawn by experts for a particular taxon (as for the mammal and amphibian distribution data used in this study). However, range maps are only available for a limited number of organisms, including terrestrial vertebrates[43]and a few plant groups[27]. Range maps usually have a continental or global extent, but they are analysed at a coarse resolution (e.g. 1º × 1º grid cells) because they tend to predict false presences at finer resolution due to variation in landscapes and habitats. (ii) Species inventories, which are lists of species in a given area which allow reliable comparisons of species richness, endemism and other dimensions of biodiversity among regions and globally[30]. Their spatial resolution (area covered) varies, typically from 0.5 hectare plots to national parks, but is finer than those of range maps. (iii) Geo-referenced species occurrences from natural history collections and observations, which comprise hundreds of millions of records in public databases (such as gbif.org, mol.org and mountainbiodiversity.org). This data source has the finest resolution (with uncertainty in the range of meters to kilometres), but is prone to uneven sampling activity[103] and several sources of bias[104]. Species occurrence records are the basis for species distribution models (SDMs), which estimate the geographic distribution of individual species based on environmental associations[105].

Figure B2 | The relation among alpha, beta and gamma diversity in mountain systems. In each of the mountains depicted, an elevational transect containing six inventory plots yields six measures of alpha-diversity (lower graph). When the species found among plots of the same transect vary a lot (high beta; red transect), the total diversity estimated for the mountain (gamma diversity) is generally also high (upper graph).

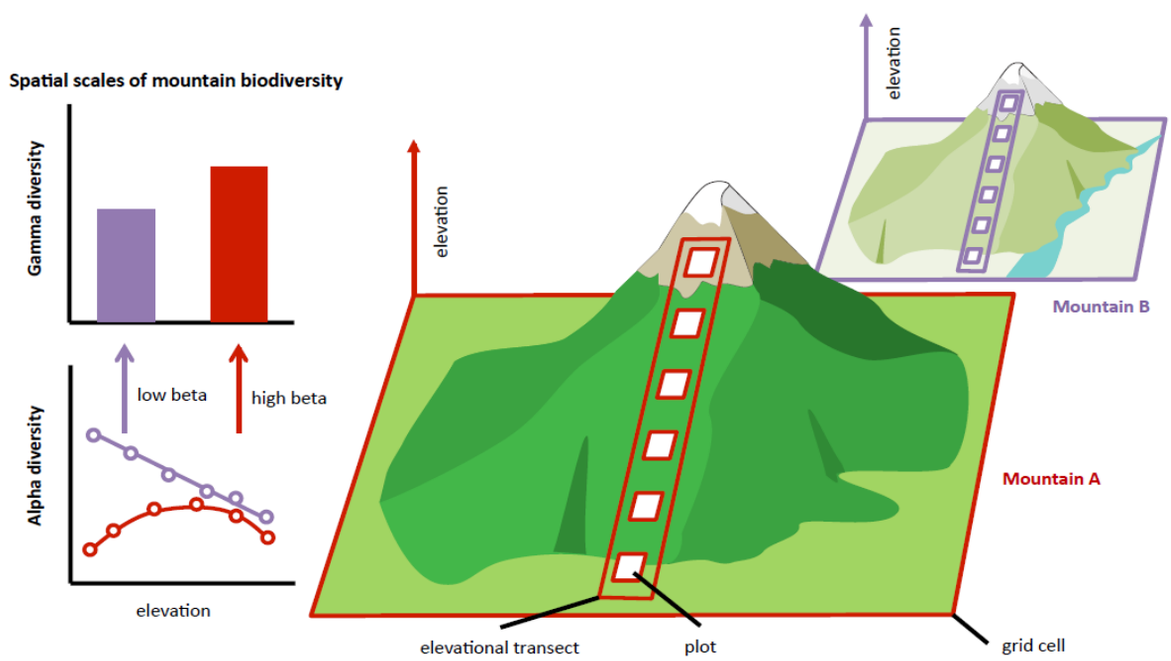

Figure 1 | The world's mountains and centres of biodiversity. a, Montane regions as depicted from a high-resolution (ca. 1 km) digital elevation model of the Earth[79]. The Greenland ice sheet is plotted in white. b, Biodiversity illustrated as the number of species of terrestrial vertebrates (birds, mammals and amphibians) present in 1º grid cells[80,18]. Maps areplotted with natural-breaks classification and a World Geodetic System projection (WGS 1984).

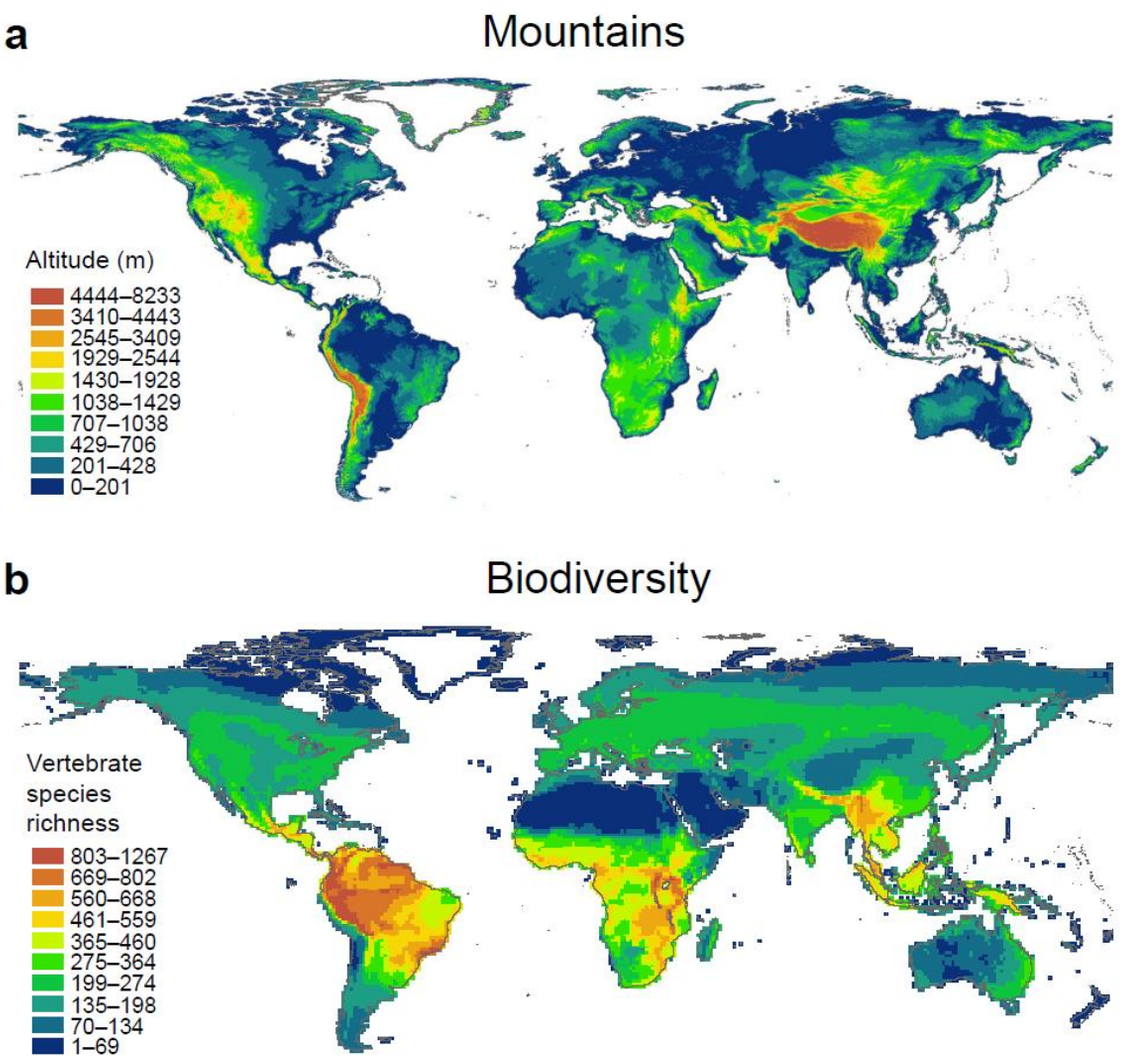

Figure 2 | Global determinants of biodiversity across the world's mountains. a, Relative importance (standardised coefficients) of predictor variables from the global multi-predictor model across 1° grid cells within mountain regions, relating species richness of vertebrates to climatic (blue) and geological (green) predictor variables (the direction of effect is indicated as + or -). **b–g** Partial residual plots of predictor variables from the same model. Partial residuals represent the relationship between a response and a predictor variable when all other predictor variables in the model are statistically controlled. Predictor variables are explained in the inset and in Table 1.

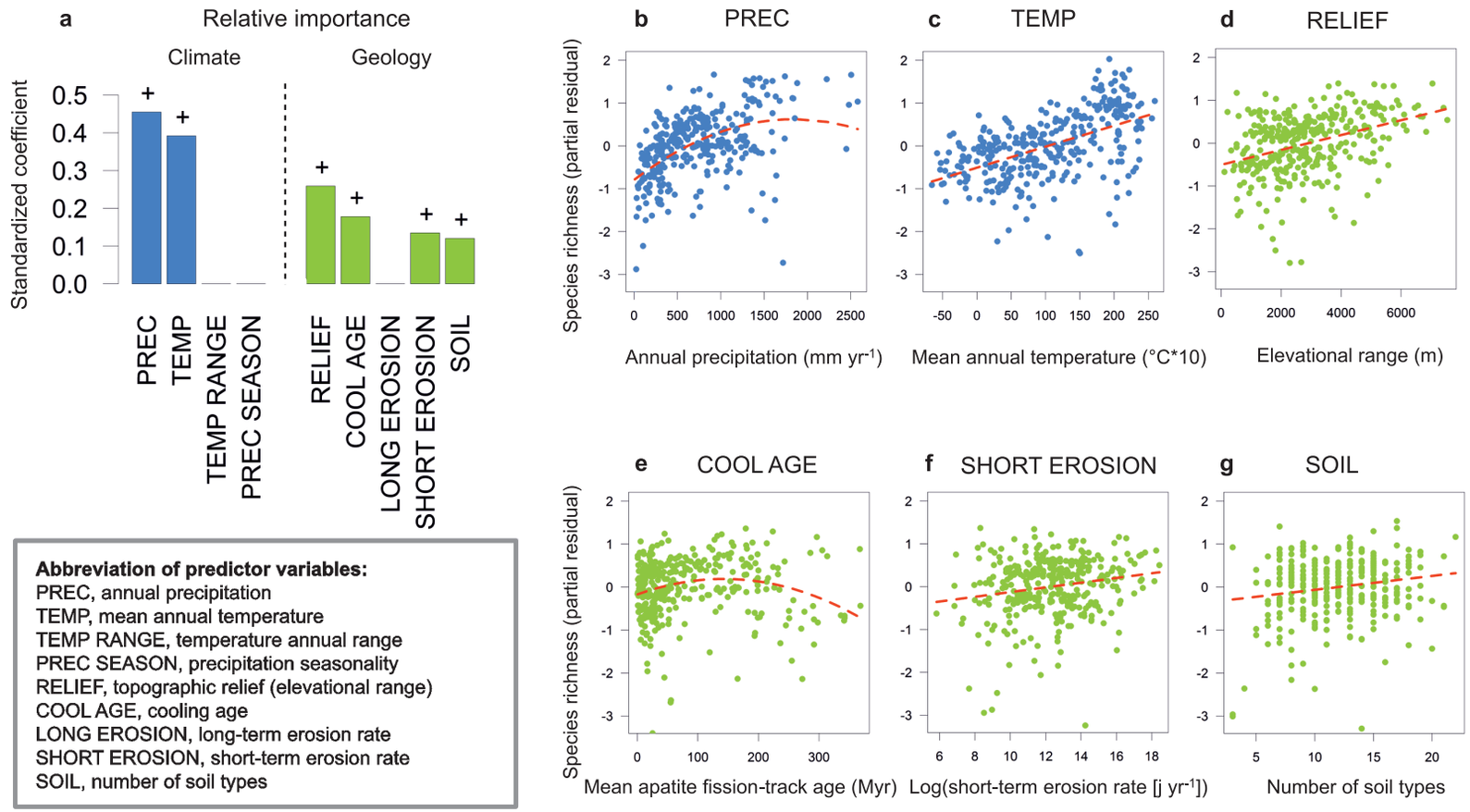

Figure 3 | Regional determinants of mountain biodiversity. a, Variation in species richness of terrestrial vertebrates for all included grid cells (n = 327) and the eight mountain regions summarised in this study. b–e Results from analyses of four mountain regions with sufficient sample sizes (>30 grid cells), illustrating the relative importance of each variable, as well as the relation between the predominant geological variable and richness. b, North America; c, The Andes; d, Eastern Africa; e, High Asia. For High Asia, cooling age and long-term erosion rate have equal predictive power and only one is shown. See Figure 2 and Table 1 for abbreviations of predictor variables.

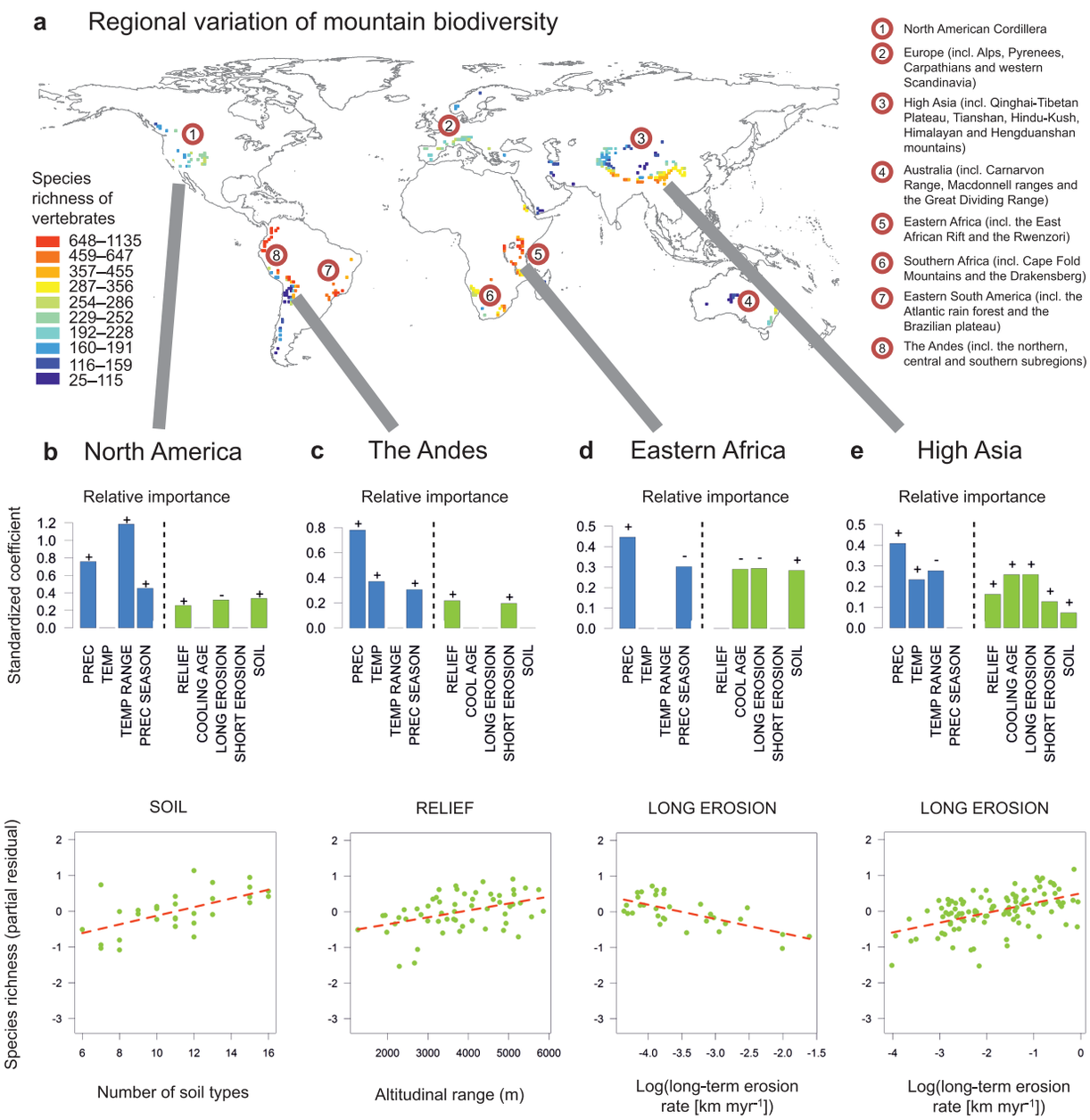
a Regional variation of mountain biodiversity
Species richness of vertebrates
648–1135
459–647
357–455
287–356
254–286
229–252
192–228
160–191
116–159
25–115
1 North American Cordillera
2 Europe (incl. Alps, Pyrenees, Carpathians and western Scandinavia)
3 High Asia (incl. Qinghai-Tibetan Plateau, Tianshan, Hindu-Kush, Himalayan and Hengduanshan mountains)
4 Australia (incl. Carnarvon Range, Macdonnell ranges and the Great Dividing Range)
5 Eastern Africa (incl. the East African Rift and the Rwenzori)
6 Southern Africa (incl. Cape Fold Mountains and the Drakensberg)
7 Eastern South America (incl. the Atlantic rain forest and the Brazilian plateau)
8 The Andes (incl. the northern, central and southern subregions)
b North America
c The Andes
d Eastern Africa
e High Asia
Relative importance
Standardized coefficient
PREC
TEMP
TEMP RANGE
PREC SEASON
RELIEF
COOLING AGE
COOL AGE
LONG EROSION
SHORT EROSION
SOIL
Species richness (partial residual)
Number of soil types
Altitudinal range (m)
Log(long-term erosion rate [km myr-1])

Figure 4 | Mountain building and biodiversity. a, Key mountain building processes. (Modified from[106]). **b**, Typical vegetation zones along elevational gradients (illustrated with an example from the Andes[81]). **c**, Four main patterns of species richness change along elevational gradients (red: decreasing trend; blue: low-elevation plateau; yellow: low-elevation plateau with a mid-peak; brown: midpeak; modified from[46]. **d**, Speciation increases species richness, e.g. through genetic isolation of populations and adaptation to different soil types or vegetation zones at higher elevations[9]. Surface uplift leads to the formation of new habitats which can trigger speciation and the accumulation of local endemics. **e**, Extinction of species (illustrated with red crosses) decreases species richness, e.g. when mountain habitats disappear due to erosion, landslides or volcanic eruptions, or when global warming drives species upslope (mountain top extinctions). **f**, Dispersal increases species richness when new immigrant species arrive from other mountain systems. Such immigrant lineages can then undergo local speciation which further increases species richness[9].

a) Mountain building

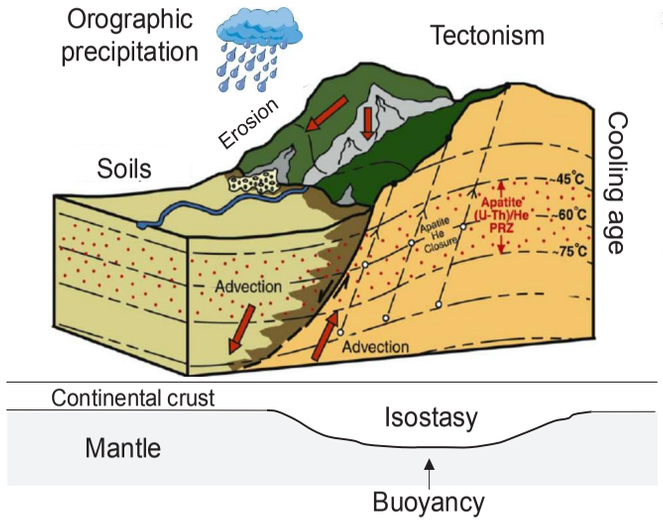

b) Vegetation zones

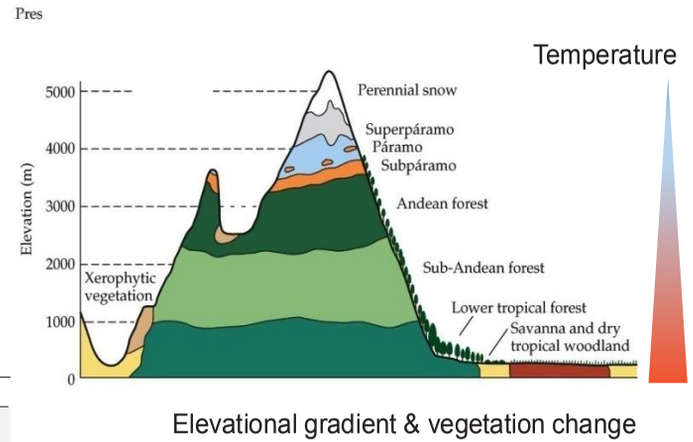

Elevational gradient & vegetation change

c) Biodiversity

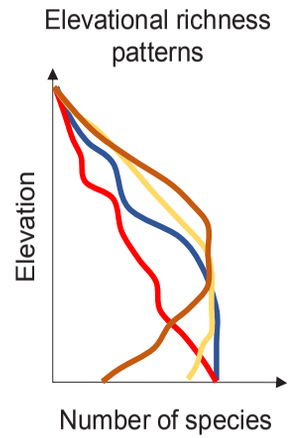

d) Speciation

e) Extinction

f) Dispersal

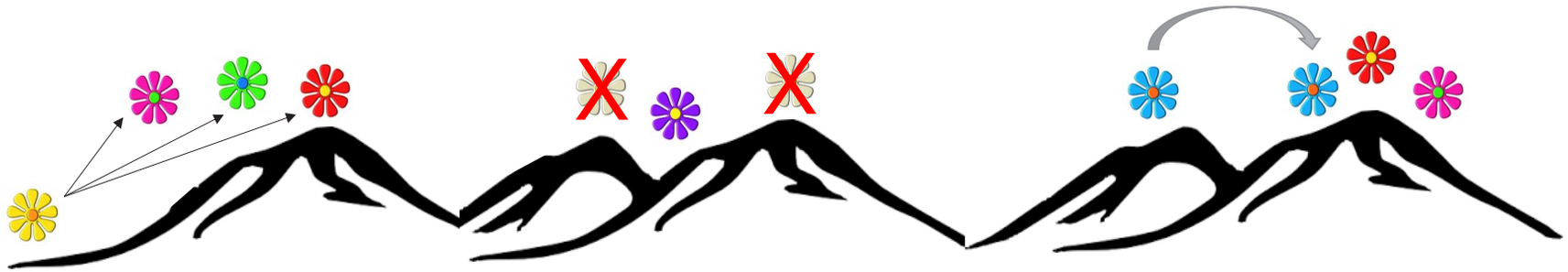

Table 1 Climatic and geological predictor variables used for analysing vertebrate species richness across the world's mountains.

Abbreviation	Description*	Unit
Climate		
PREC	Annual precipitation	mm $year^{-1}$
TEMP	Mean annual temperature	°C × 10
TEMP RANGE	Temperature annual range (maximum temperature of warmest month minus minimum temperature of coldest month)	°C × 10
PREC SEASON	Precipitation seasonality: coefficient of variation of monthly values	mm
Geology		
RELIEF	Topographic relief: range in elevation	m
COOL AGE	Cooling age: mean value of apatite fission-track ages	myr
LONG EROSION	Long-term erosion rate derived from apatite fission-track values	km myr^{-1}
SHORT EROSION	Short-term erosion rate measured as total stream power index weighted with precipitation data	W m^{-1}
SOIL	Number of soil types	count

*Sources of data are provided in Supplementary Table S1.

REFERENCES

1. Badgley, C. Tectonics, topography, and mammalian diversity. *Ecography* **33,** 220–231 (2010).
2. Fjeldså, J., Bowie, R. C. K. & Rahbek, C. The Role of Mountain Ranges in the Diversification of Birds. *Annual Review of Ecology, Evolution, and Systematics* **43,** 249–265 (2012).
3. Badgley, C. *et al.* Biodiversity and Topographic Complexity: Modern and Geohistorical Perspectives. *Trends in Ecology & Evolution* **32,** 211–226 (2017).
4. Hoorn, C., Mosbrugger, V., Mulch, A. & Antonelli, A. Biodiversity from mountain building. *Nature Geosci* **6,** 154–154 (2013).
5. Antonelli, A. Biodiversity: Multiple origins of mountain life. *Nature* **524,** 300–301 (2015).
6. Eronen, J. T., Janis, C. M., Chamberlain, C. P. & Mulch, A. Mountain uplift explains differences in Palaeogene patterns of mammalian evolution and extinction between North America and Europe. *Proc. R. Soc. B* **282,** 20150136 (2015).
7. Ebersbach, J. *et al.* In and out of the Qinghai-Tibet Plateau: divergence time estimation and historical biogeography of the large arctic-alpine genus Saxifraga L. *J. Biogeogr.* n/a-n/a (2016). doi:10.1111/jbi.12899
8. Favre, A. *et al.* The role of the uplift of the Qinghai-Tibetan Plateau for the evolution of Tibetan biotas. *Biol Rev* **90,** 236–253 (2015).
9. Merckx, V. S. F. T. *et al.* Evolution of endemism on a young tropical mountain. *Nature* **524,** 347–350 (2015).
10. Chaboureau, A.-C., Sepulchre, P., Donnadieu, Y. & Franc, A. Tectonic-driven climate change and the diversification of angiosperms. *Proceedings of the National Academy of Sciences* **111,** 14066–14070 (2014).
11. Salazar, L. F. & Nobre, C. A. Climate change and thresholds of biome shifts in Amazonia. *Geophys. Res. Lett.* **37,** L17706 (2010).
12. Kutzbach, J. E., Prell, W. L. & Ruddiman, W. F. Sensitivity of Eurasian Climate to Surface Uplift of the Tibetan Plateau. *The Journal of Geology* **101,** 177–190 (1993).
13. Hay, W., Soeding, E., DeConto, R. & Wold, C. The Late Cenozoic uplift - climate change paradox. *International Journal of Earth Sciences* **91,** 746–774 (2002).
14. Mix, H. T., Winnick, M. J., Mulch, A. & Page Chamberlain, C. Grassland expansion as an instrument of hydrologic change in Neogene western North America. *Earth and Planetary Science Letters* **377–378,** 73–83 (2013).
15. Mulch, A. & Chamberlain, C. P. Earth science: The rise and growth of Tibet. *Nature* **439,** 670–671 (2006).
16. Rowley, D. B. & Garzione, C. N. Stable Isotope-Based Paleoaltimetry. *Annual Review of Earth and Planetary Sciences* **35,** 463–508 (2007).
17. Herman, F. *et al.* Worldwide acceleration of mountain erosion under a cooling climate. *Nature* **504,** 423–426 (2013).
18. IUCN. The IUCN red list of threatened species. Version 2013. (2013). http://www.iucnredlist.org
19. Hedges, S. B., Dudley, J. & Kumar, S. TimeTree: a public knowledge-base of divergence times among organisms. *Bioinformatics* **22,** 2971–2972 (2006).
20. Morlon, H. Phylogenetic approaches for studying diversification. *Ecol Lett* **17,** 508–525 (2014).
21. Silvestro, D., Schnitzler, J., Liow, L. H., Antonelli, A. & Salamin, N. Bayesian Estimation of Speciation and Extinction from Incomplete Fossil Occurrence Data. *Syst Biol* **63,** 349–367 (2014).
22. Fritz, S. A. *et al.* Diversity in time and space: wanted dead and alive. *Trends in Ecology & Evolution* **28,** 509–516 (2013).
23. Craw, D., Upton, P., Burridge, C. P., Wallis, G. P. & Waters, J. M. Rapid biological speciation driven by tectonic evolution in New Zealand. *Nature Geosci* **9,** 140–144 (2016).
24. Currie, D. J. Energy and Large-Scale Patterns of Animal- and Plant-Species Richness. *The American Naturalist* **137,** 27–49 (1991).
25. Hawkins, B. A. *et al.* Energy, water, and broad-scale geographical patterns of species richness. *Ecology* **84,** 3105–3117 (2003).
26. Kerr, J. T. & Packer, L. Habitat heterogeneity as a determinant of mammal species richness in high-energy regions. *Nature* **385,** 252–254 (1997).
27. Kreft, H., Sommer, J. H. & Barthlott, W. The significance of geographic range size for spatial diversity patterns in Neotropical palms. *Ecography* **29,** 21–30 (2006).
28. Körner, C. Why are there global gradients in species richness? mountains might hold the answer. *Trends in Ecology & Evolution* **15,** 513–514 (2000).
29. Stein, A., Gerstner, K. & Kreft, H. Environmental heterogeneity as a universal driver of species richness across taxa, biomes and spatial scales. *Ecology Letters* **17,** 866–880 (2014).
30. Kreft, H. & Jetz, W. Global patterns and determinants of vascular plant diversity. *PNAS* **104,** 5925–5930 (2007).

31. Ricklefs, R. E. A comprehensive framework for global patterns in biodiversity. *Ecology Letters* **7,** 1–15 (2004).
32. Mittelbach, G. G. *et al.* Evolution and the latitudinal diversity gradient: speciation, extinction and biogeography. *Ecology Letters* **10,** 315–331 (2007).
33. Kissling, W. D. *et al.* Cenozoic imprints on the phylogenetic structure of palm species assemblages worldwide. *PNAS* **109,** 7379–7384 (2012).
34. Araújo, M. B. *et al.* Quaternary climate changes explain diversity among reptiles and amphibians. *Ecography* **31,** 8–15 (2008).
35. Kissling, W. D. *et al.* Quaternary and pre-Quaternary historical legacies in the global distribution of a major tropical plant lineage: Historical legacies in tropical biodiversity. *Global Ecology and Biogeography* **21,** 909–921 (2012).
36. Mayhew, P. J., Bell, M. A., Benton, T. G. & McGowan, A. J. Biodiversity tracks temperature over time. *PNAS* **109,** 15141–15145 (2012).
37. Blach-Overgaard, A., Kissling, W. D., Dransfield, J., Balslev, H. & Svenning, J.-C. Multimillion-year climatic effects on palm species diversity in Africa. *Ecology* **94,** 2426–2435 (2013).
38. Mannion, P. D., Upchurch, P., Benson, R. B. J. & Goswami, A. The latitudinal biodiversity gradient through deep time. *Trends in Ecology & Evolution* **29,** 42–50 (2014).
39. Finarelli, J. A. & Badgley, C. Diversity dynamics of Miocene mammals in relation to the history of tectonism and climate. *Proceedings of the Royal Society of London B: Biological Sciences* **277,** 2721–2726 (2010).
40. Hoorn, C. *et al.* Amazonia Through Time: Andean Uplift, Climate Change, Landscape Evolution, and Biodiversity. *Science* **330,** 927–931 (2010).
41. Jetz, W. & Rahbek, C. Geographic Range Size and Determinants of Avian Species Richness. *Science* **297,** 1548–1551 (2002).
42. Rahbek, C. *et al.* Predicting continental-scale patterns of bird species richness with spatially explicit models. *Proceedings of the Royal Society of London B: Biological Sciences* **274,** 165–174 (2007).
43. Grenyer, R. *et al.* Global distribution and conservation of rare and threatened vertebrates. *Nature* **444,** 93–96 (2006).
44. McCain, C. M. Elevational gradients in diversity of small mammals. *Ecology* **86,** 366–372 (2005).
45. Field, R. *et al.* Spatial species-richness gradients across scales: a meta-analysis. *Journal of Biogeography* **36,** 132–147 (2009).
46. McCain, C. M. & Grytnes, J.-A. *Elevational Gradients in Species Richness*. (John Wiley & Sons, 2010). doi:10.1002/9780470015902.a0022548
47. Strecker, M. R. *et al.* Tectonics and Climate of the Southern Central Andes. *Annual Review of Earth and Planetary Sciences* **35,** 747–787 (2007).
48. Mulch, A., Uba, C. E., Strecker, M. R., Schoenberg, R. & Chamberlain, C. P. Late Miocene climate variability and surface elevation in the central Andes. *Earth and Planetary Science Letters* **290,** 173–182 (2010).
49. Poulsen, C. J., Ehlers, T. A. & Insel, N. Onset of Convective Rainfall During Gradual Late Miocene Rise of the Central Andes. *Science* **328,** 490–493 (2010).
50. Holt, B. G. *et al.* An Update of Wallace's Zoogeographic Regions of the World. *Science* **339,** 74–78 (2013).
51. Badgley, C. & Fox, D. L. Ecological biogeography of North American mammals: species density and ecological structure in relation to environmental gradients. *Journal of Biogeography* **27,** 1437–1467 (2000).
52. Kent-Corson, M. L., Barnosky, A. D., Mulch, A., Carrasco, M. A. & Chamberlain, C. P. Possible regional tectonic controls on mammalian evolution in western North America. *Palaeogeography, Palaeoclimatology, Palaeoecology* **387,** 17–26 (2013).
53. Luebert, F. & Weigend, M. Phylogenetic insights into Andean plant diversification. *Front. Ecol. Evol* **2,** 1–17 (2014).
54. Antonelli, A., Nylander, J. A. A., Persson, C. & Sanmartín, I. Tracing the impact of the Andean uplift on Neotropical plant evolution. *PNAS* **106,** 9749–9754 (2009).
55. Mutke, J., Jacobs, R., Meyers, K., Henning, T. & Weigend, M. Diversity patterns of selected Andean plant groups correspond to topography and habitat dynamics, not orogeny. *Frontiers in Genetics* **5,** (2014).
56. Hughes, C. & Eastwood, R. Island radiation on a continental scale: Exceptional rates of plant diversification after uplift of the Andes. *PNAS* **103,** 10334–10339 (2006).
57. Diazgranados, M. & Barber, J. C. Geography shapes the phylogeny of frailejones (Espeletiinae Cuatrec., Asteraceae): a remarkable example of recent rapid radiation in sky islands. *PeerJ* **5,** e2968 (2017).
58. Burgess, N. D. *et al.* The biological importance of the Eastern Arc Mountains of Tanzania and Kenya. *Biological Conservation* **134,** 209–231 (2007).
59. Moucha, R. & Forte, A. M. Changes in African topography driven by mantle convection. *Nature Geoscience* **4,** 707–712 (2011).

60. Kaufmann, G. & Romanov, D. Landscape evolution and glaciation of the Rwenzori Mountains, Uganda: Insights from numerical modeling. *Geomorphology* **138,** 263–275 (2012).
61. Bauer, F. U. *et al.* Tracing the exhumation history of the Rwenzori Mountains, Albertine Rift, Uganda, using low-temperature thermochronology. *Tectonophysics* **599,** 8–28 (2013).
62. Fjeldså, J. & Lovett, J. C. Geographical patterns of old and young species in African forest biota: the significance of specific montane areas as evolutionary centres. *Biodiversity and Conservation* **6,** 325–346 (1997).
63. Yan, Y., Yang, X. & Tang, Z. Patterns of species diversity and phylogenetic structure of vascular plants on the Qinghai-Tibetan Plateau. *Ecology and Evolution* **3,** 4584–4595 (2013).
64. Jacques, F. M. B. *et al.* Quantitative reconstruction of the Late Miocene monsoon climates of southwest China: A case study of the Lincang flora from Yunnan Province. *Palaeogeography, Palaeoclimatology, Palaeoecology* **304,** 318–327 (2011).
65. Lei, F., Qu, Y., Song, G., Alström, P. & Fjeldså, J. The potential drivers in forming avian biodiversity hotspots in the East Himalaya-Mountains of Southwest China. *Integrative Zoology* n/a-n/a (2014). doi:10.1111/1749-4877.12121
66. Benton, M. J. The Red Queen and the Court Jester: species diversity and the role of biotic and abiotic factors through time. *Science* **323,** 728–732 (2009).
67. Graham, C. H. *et al.* The origin and maintenance of montane diversity: integrating evolutionary and ecological processes. *Ecography* **37,** 711–719 (2014).
68. Whittaker, R. J., Triantis, K. A. & Ladle, R. J. A general dynamic theory of oceanic island biogeography. *Journal of Biogeography* **35,** 977–994 (2008).
69. Price, T. D. *et al.* Niche filling slows the diversification of Himalayan songbirds. *Nature* **509,** 222–225 (2014).
70. Hughes, C. E. & Atchison, G. W. The ubiquity of alpine plant radiations: from the Andes to the Hengduan Mountains. *New Phytol* **207,** 275–282 (2015).
71. Morueta-Holme, N. *et al.* Strong upslope shifts in Chimborazo's vegetation over two centuries since Humboldt. *PNAS* **112,** 12741–12745 (2015).
72. Sandel, B. *et al.* The Influence of Late Quaternary Climate-Change Velocity on Species Endemism. *Science* **334,** 660–664 (2011).
73. Beck, J. & Kitching, I. J. Drivers of moth species richness on tropical altitudinal gradients: a cross-regional comparison. *Global Ecology and Biogeography* **18,** 361–371 (2009).
74. Barnagaud, J.-Y. *et al.* Ecological traits influence the phylogenetic structure of bird species co-occurrences worldwide. *Ecol Lett* **17,** 811–820 (2014).
75. Díaz, S. *et al.* Functional traits, the phylogeny of function, and ecosystem service vulnerability. *Ecol Evol* **3,** 2958–2975 (2013).
76. Jetz, W., Thomas, G. H., Joy, J. B., Hartmann, K. & Mooers, A. O. The global diversity of birds in space and time. *Nature* **491,** 444–448 (2012).
77. Baker, P. A. *et al.* The emerging field of geogenomics: Constraining geological problems with genetic data. *Earth-Science Reviews* **135,** 38–47 (2014).
78. Lagomarsino, L. P., Condamine, F. L., Antonelli, A., Mulch, A. & Davis, C. C. The abiotic and biotic drivers of rapid diversification in Andean bellflowers (Campanulaceae). *New Phytol* **210,** 1430–1442 (2016).
79. Farr, T. G. *et al.* The Shuttle Radar Topography Mission. *Reviews of Geophysics* **45,** (2007).
80. Rahbek, C., Hansen, L. A. & Fjeldså, J. One degree resolution database of the global distribution of birds. (2012).
81. Van der Hammen, T. The Pleistocene Changes of Vegetation and Climate in Tropical South America. *Journal of Biogeography* **1,** 3–26 (1974).
82. Molnar, P. & England, P. Late Cenozoic uplift of mountain ranges and global climate change: chicken or egg? *Nature* **346,** 29–34 (1990).
83. Chamberlain, C. P., Poage, M. A., Craw, D. & Reynolds, R. C. Topographic development of the Southern Alps recorded by the isotopic composition of authigenic clay minerals, South Island, New Zealand. *Chemical Geology* **155,** 279–294 (1999).
84. Rowley, D. B., Pierrehumbert, R. T. & Currie, B. S. A new approach to stable isotope-based paleoaltimetry: implications for paleoaltimetry and paleohypsometry of the High Himalaya since the Late Miocene. *Earth and Planetary Science Letters* **188,** 253–268 (2001).
85. Mulch, A. Stable isotope paleoaltimetry and the evolution of landscapes and life. *Earth and Planetary Science Letters* **433,** 180–191 (2016).
86. Garzione, C. N. *et al.* Rise of the Andes. *Science* **320,** 1304–1307 (2008).
87. Campani, M., Mulch, A., Kempf, O., Schlunegger, F. & Mancktelow, N. Miocene paleotopography of the Central Alps. *Earth and Planetary Science Letters* **337–338,** 174–185 (2012).

88. Gébelin, A. *et al.* The Miocene elevation of Mount Everest. *Geology* G34331.1 (2013). doi:10.1130/G34331.1
89. Chamberlain, C. P. *et al.* The Cenozoic climatic and topographic evolution of the western North American Cordillera. *American Journal of Science* **312,** 213–262 (2012).
90. Rowley, D. B. & Currie, B. S. Palaeo-altimetry of the late Eocene to Miocene Lunpola basin, central Tibet. *Nature* **439,** 677–681 (2006).
91. Ruddiman, W. F. & Kutzbach, J. E. Forcing of late Cenozoic northern hemisphere climate by plateau uplift in southern Asia and the American west. *J. Geophys. Res.* **94,** 18409–18427 (1989).
92. Raymo, M. E. & Ruddiman, W. F. Tectonic forcing of late Cenozoic climate. *Nature* **359,** 117–122 (1992).
93. Licht, A. *et al.* Asian monsoons in a late Eocene greenhouse world. *Nature* **513,** 501–506 (2014).
94. Reiners, P. W. & Brandon, M. T. Using Thermochronology to Understand Orogenic Erosion. *Annual Review of Earth and Planetary Sciences* **34,** 419–466 (2006).
95. Herman, F. & Champagnac, J.-D. Plio-Pleistocene increase of erosion rates in mountain belts in response to climate change. *Terra Nova* **28,** 2–10 (2016).
96. Champagnac, J.-D., Valla, P. G. & Herman, F. Late-Cenozoic relief evolution under evolving climate: A review. *Tectonophysics* **614,** 44–65 (2014).
97. Heywood, V. H. *Global biodiversity assessment*. (Cambridge ; New York, NY, USA : Cambridge University Press, 1995).
98. Purvis, A. & Hector, A. Getting the measure of biodiversity. *Nature* **405,** 212–219 (2000).
99. Webb, C. O., Ackerly, D. D., McPeek, M. A. & Donoghue, M. J. Phylogenies and Community Ecology. *Annual Review of Ecology and Systematics* **33,** 475–505 (2002).
100. Mace, G. M., Gittleman, J. L. & Purvis, A. Preserving the Tree of Life. *Science* **300,** 1707–1709 (2003).
101. Whittaker, R. H. Evolution and Measurement of Species Diversity. *Taxon* **21,** 213–251 (1972).
102. Tuomisto, H. A diversity of beta diversities: straightening up a concept gone awry. Part 1. Defining beta diversity as a function of alpha and gamma diversity. *Ecography* **33,** 2–22 (2010).
103. Yang, W., Ma, K. & Kreft, H. Environmental and socio-economic factors shaping the geography of floristic collections in China. *Global Ecology and Biogeography* **23,** 1284–1292 (2014).
104. Meyer, C., Kreft, H., Guralnick, R. & Jetz, W. Global priorities for an effective information basis of biodiversity distributions. *Nat Commun* **6,** 8221 (2015).
105. Franklin, J. & Miller, J. A. *Mapping species distributions: spatial inference and prediction*. (Cambridge University Press, 2009).
106. Ehlers, T. A. & Farley, K. A. Apatite (U–Th)/He thermochronometry: methods and applications to problems in tectonic and surface processes. Earth and Planetary Science Letters 206, 1–14 (2003).

METHODS

Distribution data

All distribution data of terrestrial vertebrates were compiled at 1º × 1º latitude-longitude grid cells[1]. The global range maps of virtually all amphibians (6086 species) and non-marine mammals (5148 species) were based on IUCN Global Assessment distributional data for native geographic ranges[2,3]. Breeding distributions for 9650 non-pelagic species of birds were extracted from a comprehensive global distribution database for all birds[4]. Geographic ranges represent a conservative extent-of-occurrence of the breeding areas of species, based on museum specimens, published sight records, expert opinion, and spatial distributions of habitats.

Predictor variables

We used a total of nine predictor variables (Table 1 & Table S1) which we considered of potential relevance in predicting species richness of vertebrates in the world's mountains. The variables reflected climate (annual precipitation, mean annual temperature, temperature annual range, and precipitation seasonality) and geology (topographic relief, cooling age, long-term erosion rate, short-term erosion rate, and number of different soil types). These predictor variables are described in more detail below, and an overview with data sources is given in Supplementary Table S1.

Climate

Climate variables (PREC, TEMP, TEMP RANGE, PREC SEASON; Table S1) were extracted from WORLDCLIM[5] (version 1.4, release 3, available at http://www.worldclim.org/) as mean values per 1º × 1º grid cells using ArcGIS 10.3[6].

Topographic relief

To quantify topographic heterogeneity, we measured relief as elevational range (RELIEF). We used the zonal statistics in the Spatial Analyst extension of ArcGIS version 10.3[6] and obtained the elevational range (maximum minus minimum altitude) in meters within each 1º × 1º grid cell. Elevational data were available from the SRTM database at 90 m resolution (version 4.1)[7].

Cooling ages

The cooling ages (COOL AGE; Table S1) are synonymous with apatite fission track (AFT) ages. Cooling ages provide an estimate of the time since a rock went through a given closure temperature[8] (Dodson, 1973) as it travels through the Earth's crust. Based on knowledge of the Earth's crust thermal state, or using a thermal model, these can be converted into exhumation/denudation rates at the time scale of the apparent age. In particular, cooling ages yield information on the timing since a rock passed through the 2–5 km window (in normal conditions, which is equivalent to c. 60°–120°C temperature) during cooling, as a result of upper crustal tectonic and/or surface processes. AFTs are formed when charged particles are released by the spontaneous nuclear fission of uranium 238 in apatite crystals. The highly-charged particles released by the fission reaction damage the lattice of apatite crystals. The damage appears as linear features which are referred to as fission tracks. The number of fission tracks in a crystal can then be used to measure the time since the formation of the apatite grains. We used the global AFT dataset from Herman *et al.* (2013)[9] and compared the AFT estimates with the South American dataset from Hoorn *et al.* (2010)[10], completing the data where they were missing from Herman *et al.* (2013)[9]. In addition, the AFT database was extended by taking into account other previous work[11,12,13,14,15,16] which had not been

included in the Herman *et al.* (2013)[9] dataset. Most ages were processed using the 'External Detector Method[17,18,19,20,21,22].It is worth stressing here that cooling ages may not necessarily be associated with recent/ongoing tectonic or erosional events. We included cooling age as a proxy for when at least part of a mountain range was formed (but not necessarily its surface). This variable is thus linked to above-ground geophysical processes that could affect biodiversity.

Erosion rates

We calculated erosion rates at two different timescales. The first one reflects long-term erosion (LONG EROSION), i.e. acting on geological (>1 million-year) timescales, which are defined as the average rate of erosion for a period of time >100 ka. The second variable reflects short-term erosion (SHORT EROSION), which is measured on a human (1–10 yr) timescale and is eventually overridden by long-term erosion.

We used a global compilation of thermochronometric data to estimate LONG EROSION, applying two independent methods. First, steady state long-term erosion rates were estimated using the software Age2edot[23], referred to below as Brandon's method. Second, we used a formal inversion approach designed to interpret spatially distributed data [24,9], referred to below as Fox-Herman's method. We acknowledge that there are several general limitations when using cooling ages to infer erosion rates and how they vary with time. For instance, erosion rates derived from a single thermochronometer heavily depend on knowledge of the Earth's crust thermal field. In most cases, the thermal field is poorly known and a thermal model must therefore be used. This limitation can in part be circumvented by collecting samples at different elevations (in which case the slope of the relationship between age and elevation provides an estimate of the exhumation rate) or using thermochronometers with different closure temperature. Furthermore, a thermochronometric age only provides an estimate of the erosion rate integrated over the time defined by its apparent age, and care must be taken when comparing observations made across different timescales.

With Brandon's method, Age2edot solves the heat transfer equation and enables to convert an age into an erosion rate, assuming that erosion rate has remained steady through time. The thermal field is represented by the steady-state solution for a crustal block with a thickness L (km), a thermal diffusivity κ (km^2 Myr^{-1}), a uniform internal heat production HT (ºC Ma^{-1}), a steady surface temperature T_s (ºC) and an estimate of the near-surface thermal gradient for no erosion (ºC km^{-1}). These thermal parameters are usually estimated, at least in part, from heat flow studies. This model does not account for transient thermal effects[25] or the 3-D effects of topography[26]. To illustrate how this method works, Fig. S7 shows a hypothetical example of how long-term erosion rates are related to AFT age estimates using Age2edot (thick black line). The thin black lines show that an AFT age of 1 Myr corresponds to a long-term cooling rate of 1.8 km Myr^{-1}. The method was applied to the AFT data only. Regionally available parameters as available from different scientific publications were used in the model. A summary with the list of references from which regional parameters were derived is provided in Supplementary Table S2.

The second method, i.e. the Fox-Herman's method, is described in detail in Fox et al. (2014)[24] and Herman et al. (2013)[9]. The objective of this approach is to formally invert spatially distributed thermochronometric data into maps of erosion rates back in time. This method has some advantages in comparison to Brandon's method. It exploits the information contained in both age-elevation profiles and multi-thermochronometric systems strategies, and it accounts for the conductive effects of topography on the underlying isotherms. The method relies on the fact that cooling age (τ) and erosion rates (□) can be related through the following integral:

$$\int_0^{\tau} \dot{\varepsilon}(t)dt = z_c \tag{1}$$

where z_c is the closure depth, i.e., the depth of the closure temperature T_c. A one-dimensional thermal model that solves the heat transfer equation and includes a spectral solution for the effects of topography on the shape of the isotherms enables to estimates the thermal field. The depth of closure temperature is computed by extracting the cooling history of each sample and using the Dobson's equation[25]. Here four thermochronometric systems were included, as explained in Herman et al. (2013)[9]. To obtain a useful numerical solution for equation (1), Fox et al (2014)[24] and Herman et al (2013)[9] discretise the integral, in terms of a summation, in which erosion rate is parameterised as a piecewise constant function over fixed time intervals. A thermochronometric age is thus represented by a linear equation, and a suite of n thermochronometric ages, of this way becomes a linear system of independent equations:

$$A\dot{\varepsilon} = z_c$$

In this last, z_c is the vector with n different closure depths, $\dot{\varepsilon}$ is a vector with unknown erosion rates and A is a matrix of cooling ages. Using the regularization method Fox et al (2013) solved the under-determined inverse problem. They suppose that erosion rates are correlated in space by means of a covariance matrix C. This last matrix is constructed for all time intervals using the horizontal distance (d) between data points (i,j) and the correlation function:

$$C_{ij} = \sigma_e^2 e^{-\frac{d}{\lambda}}$$

where λ is a specified correlation length (30 km). The solution to the inverse problem for the erosion rate $\dot{\varepsilon}$ is ([24], [9])

$$\dot{\varepsilon} = \dot{\varepsilon}_{pr} + CA^T\left(ACA^T + C_\varepsilon\right)^{-1}\left(z_c - A\dot{\varepsilon}_{pr}\right)$$

$\dot{\varepsilon}_{pr}$ is the a priori expected value for the erosion rate and C_ε is a diagonal matrix with the estimated data uncertainty.

By defining the resolution matrix R as:

$$R = CA^T\left(ACA^T + C_\varepsilon\right)^{-1}A$$

it is possible to evaluate the correction to the prior obtained model; R is integrated across the spatial dimensions.

Once the erosion rate is calculated for an area, the results were spatially interpolated on a regular grid to limit sampling biases. This was done for different time intervals 0–2 Ma, 2–4 Ma, 4–6 Ma, 6–8 Ma, 8–10 Ma, and 10–12 Ma, termed here Avg_HERMXY (where XY represents the interval X–Y). It is not possible to extend beyond 12 Ma because this introduces a considerable degree of uncertainty[9]. An average long-term erosion rate (Avg_HERMER; km/Ma) was finally calculated for the interval between 12 and 0 Ma.

Both long-term erosion rate estimates from Brandon's method and the average long-term erosion rate derived from Fox-Herman's method (Avg_HERMER) were strongly correlated (Spearman rank correlation r = 0.92). Both long-term erosion rates were tested in the multi-predictor regression models (see below) and resulted in qualitatively similar results. Moreover, all long-term erosion rates derived from Fox-Herman's method for a specific time interval (0–2 Ma, 2–4 Ma, 4–6 Ma, 6–8 Ma, 8–10 Ma, 10–12 Ma) were highly correlated

with each other and with the average long-term erosion rate from Fox-Herman's method (Spearman rank correlations $r > 0.90$). We therefore only present results using the average long-term erosion rate derived from Fox-Herman's method (Fig. 2 and Fig. 3 in main text, Supplementary Table S3).

For the calculation of short-term erosion rates (SHORT EROSION), we used the total stream power (TSP) as a proxy for present-day erosion rates. In general, predictions of the intensity of short-term erosion can be estimated using the erosion-index approach[27,28] . The erosion index can be calculated in different ways as a function of stream power, which is the rate of potential energy expenditure by flowing water. This concept has been used extensively in studies of erosion, sediment transport, and geomorphology as a measure of the erosive power of rivers and streams[29,30]. Stream power is commonly described as the capacity for flowing water to carry out geomorphic work[31]. It is a gravitational potential energy that acts as the driver for the fluvial system. This energy is converted into kinetic form through the downslope flow of water, where due to the conservation of energy; any energy lost due to falling must be converted in to another form[32]. This transformed energy is what has the potential to erode channel beds or transport sediments.

For our purpose, we calculated the short-term erosion rate as TSP following refs[27,33] as:

$$e = k A^m S^n \tag{1}$$

where e is the local incision rate, A is upstream drainage area (used as a proxy of discharge), S is local slope, and m, n and k are constants. The parameter k is mainly related to bedrock erodability. Assuming that the lithology for different areas is uniform (i.e, $k = 1$), we incorporated spatial variations in precipitation P in order to study their influence on spatial variability of the erosion potential[28].

$$TSP_P = \sum (A_P P) S, \tag{2}$$

where (A_P) is the pixel area, P is the average precipitation from 1961 to 1990, and 1998 to 2009[34,35], the summation sign implies summing along the flow-lines the area in order to calculate the flow accumulation. For the flow accumulation area (or drainage area) and the slope (S) required for the TSP_P equation (Equation 2) we used the Digital Elevation Models (DEM) from SRTM 90 m Database 4.1[7]. Slope values were calculated from the DEM in degrees using the slope function within the Spatial Analyst extension in Esri ArcGIS version 10.3. The resulting slope grid was then divided by 100 to gain slopes in m/m. The calculation of the discharge grid requires catchment area grids and discharge data. For each cell, catchment area was calculated using the flow accumulation grid. Flow accumulation represents the upstream area of a grid. Therefore, in a 1 m grid, flow accumulation is also upstream catchment area in m^2. For the 5 and 10 m grids, the square of each grid cell was calculated, resulting in a reasonable estimate of catchment area for each cell on the grid in m^2. Problems arising from the neglected measurement of diagonally contiguous pixels are considered negligible, because the DEM was corrected using the fill method in Esri ArcGIS version 10.3 before initiating calculations.

Soils

We obtained an estimate of soil heterogeneity (SOIL) per grid cell. This was calculated as the number of soil types present in each 1º × 1º grid cell as derived from a new global dataset of soil information[36]. The data was obtained by using the FTP interface (ftp.soilgrids.org) to access the 1km global grid of soil data based on the World Reference Base (WRB) for soil resources[37]. We used the variable that describes the taxonomic group of the WRB classification, version TAXGWRB_02_apr_2014. For each grid cell the number of different taxonomic soil groups was calculated using the ArcGIS Spatial Analyst tool.

Statistical analysis

Global dataset

A total of 501 grid cells were initially available for the global analysis. These grid cells contained ≥80% of area above 500 m and information on all variables, i.e. vertebrate species richness, climate, and geology. However, the number of available estimates of cooling age (i.e. COOL AGE) per grid cell varied considerably (median = 5; range: 1–252). To increase the reliability of the statistical analyses and the results, we only included those cells in the global analysis that contained ≥3 cooling age estimates per grid cell (n = 327 grid cells). These grid cells covered all major mountain regions of the world (Figure 3 in main text) and showed a large variation in vertebrate species richness, climate, and geology (Supplementary Table S3).

Regional datasets

For the regional analyses, sample sizes (i.e. number of 1º grid cells) were smaller than in the global dataset because regions represent a subset of the global pool (compare Figure 3 in the main text). Applying the same criterion as in the global dataset (i.e. including only grid cells with ≥80% of area above 500 m and with ≥3 COOL AGE estimates) allowed sample sizes to be >30 grid cells in North America (n = 32), High Asia (n = 107), the Andes (n = 57) and Eastern Africa (n = 32). We therefore implemented separate analyses similar to the global model only for those four regions.

Regression models and data transformations

We built a global as well as separate regional multivariate (ordinary least squares, OLS) regression models with vertebrate species richness as response variable and the 9 climatic and geological variables as predictors (Table 1). The response variable (vertebrate species richness) was always log-transformed in all statistical analyses. Additionally, the predictor variables long-term erosion rate and the short-term erosion rate were log-transformed to linearize relationships with the response variable, and to improve homoscedasticity. Non-linear relationships between the predictor and response variables were accounted for by adding second-order polynomials, based on the Akaike Information Criterion (AIC) and ANOVA comparisons between models with and without polynomials[38]. All predictor variables were scaled to a mean of zero and variance of 1 before the analysis to make model coefficients comparable. Residuals of models approximated a normal distribution.

We used an information-theoretic model selection based on AIC[39,38] with separate multi-predictor models for the global and the regional dataset, respectively. Before model selection, full multi-predictor models (i.e. including all nine predictor variables) were examined for multi-collinearity using Variance Inflation Factors (VIF). Predictors with high VIFs (i.e. VIF ≥ 10) were removed before model selection. Partial residual plots of each predictor variable were then examined to ensure homogeneity of variance. Using the step() function in the R software (https://www.r-project.org/), a model selection was then performed with the Akaike Information Criterion (AIC) to derive a minimum adequate model AIC[39,38],

both globally as well as separately for each region (i.e. the best model, having the smallest number of predictor variables and still a high explanatory power). For these minimum adequate models, we report the standardised coefficients of each predictor to compare the relative importance of predictor variables in explaining vertebrate species richness.

Spatial autocorrelation

We tested for the presence of spatial autocorrelation in the residuals of the multi-predictor OLS models because spatial autocorrelation could affect the interpretation of regression models[40]. We used Moran's *I* values (calculated with the four nearest neighbors) to quantify residual spatial autocorrelation. Because Moran's *I* values were significant for the OLS model residuals (Supplementary Tables S4 and S5), we implemented spatial simultaneous autoregressive (SAR) models to account for residual spatial autocorrelation [41]. SAR models supplement OLS regression with a spatial weights matrix that accounts for spatial autocorrelation in model residuals. We used a SAR model of the error type with a row-standardization for the spatial weights matrix[41]. We defined the neighborhood of the spatial weight matrix with the four nearest neighbors. For the SAR models, we quantified the explained variance of the environmental predictors (R^2_{PRED}) and the total explained variance (R^2_{FULL}) of the full SAR models (including environmental predictors and the spatial weights matrix)[41]. This was done using pseudo-R^2 values, calculated as the squared Pearson correlation between predicted and true values[41]. We present the results from the OLS models in the main text, and the results from the SAR models in the appendix (Supplementary Tables S4 and S5) because accounting for spatial autocorrelation did not qualitatively change our main results (in terms of relative importance of predictor variables). All statistical analyses were done in RStudio Version 0.99.902 (https://www.rstudio.com/).

Limitations of the analyses

Besides the general limitations in terms of data availability, completeness and biases mentioned above, we acknowledge that our analyses are correlative and that causality cannot be confidently established. We further emphasize that spatial patterns and analyses of species richness vary with spatial scale[42] and encourage future analyses at different spatial resolutions and extents, provided that appropriate biological data allow meaningful analyses at such spatial scales. Finally, we note that correlative analyses of continental and global species richness patterns have previously been criticized because they tend to give a high importance to climatic rather than topographic predictor variables when compared to macroecological null-models[43,44] or spatially explicit Monte Carlo models[45]. This is less likely a problem in our analyses because we focus on mountain regions and do not include grid cells from lowlands which are typically dominated by wide-spread species compared to grid cells in mountains where small-ranged species predominantly occur[43,45].

Methods references

1. Holt, B. G. *et al.* An Update of Wallace's Zoogeographic Regions of the World. *Science* **339,** 74–78 (2013).
2. IUCN, Conservation International & NatureServe. Global Amphibian Assessment. Available at http:// www.iucnredlist.org/amphibians. (2008).
3. IUCN. Global Mammal Assessment. Available at http:// www.iucnredlist.org/mammals. (2008).
4. Rahbek, C., Hansen, L. A. & Fjeldså, J. One degree resolution database of the global distribution of birds. (2012).
5. Hijmans, R. J., Cameron, S. E., Parra, J. L., Jones, P. G. & Jarvis, A. Very high resolution interpolated climate surfaces for global land areas. *Int. J. Climatol.* **25,** 1965–1978 (2005).
6. Environmental Systems Research Institute (ESRI). *ArcGIS Release 10.3*. (2014).

7. Jarvis, A., Reuter, H. I., Nelson, A. & Guevara, E. SRTM 90m Digital Elevation Database v4.1 | CGIAR-CSI. (2008).
8. Dodson, M. H. Closure temperature in cooling geochronological and petrological systems. *Contr. Mineral. and Petrol.* **40,** 259–274 (1973).
9. Herman, F. *et al.* Worldwide acceleration of mountain erosion under a cooling climate. *Nature* **504,** 423–426 (2013).
10. Hoorn, C. *et al.* Amazonia Through Time: Andean Uplift, Climate Change, Landscape Evolution, and Biodiversity. *Science* **330,** 927–931 (2010).
11. Dolati, A. Stratigraphy, structural geology and low-temperature thermochronology across the Makran accretionary wedge in Iran. (Eidgenössische Technische Hochschule ETH Z, 2010).
12. Rezaeian, M., Carter, A., Hovius, N. & Allen, M. B. Cenozoic exhumation history of the Alborz Mountains, Iran: New constraints from low-temperature chronometry. *Tectonics* **31,** TC2004 (2012).
13. Mbede, E. I. Tectonic development of the Rukwa rift basin in SW Tanzania. (FU Berlin, 1993).
14. Mbede, E. I. Tectonic setting and uplift analysis of the Pangani rift basin in northern Tanzania using apatite fission track thermochronology. *Tanzania Journal of Science* **27,** 23–38 (2001).
15. Biswal, T. K. & Seward, D. Tectonic implication of the Apatite Fission-track analysis of the mylonites from the Terrane Boundary Shear Zone of the Eastern Ghats Mobile Belt around Lakhna, Orissa. *Gondwana Research* **6,** 321–325 (2003).
16. Van der Beek, P., Mbede, E., Andriessen, P. & Delvaux, D. Denudation history of the Malawi and Rukwa Rift flanks (East African Rift System) from apatite fission track thermochronology. *Journal of African Earth Sciences* **26,** 363–385 (1998).
17. Gleadow, A. J. W. Fission-track dating methods: What are the real alternatives? *Nuclear Tracks* **5,** 3–14 (1981).
18. Hurford, A. J. & Green, P. F. The zeta age calibration of fission-track dating. *Chemical Geology* **41,** 285–317 (1983).
19. Green, P. F. Comparison of zeta calibration baselines for fission-track dating of apatite, zircon and sphene. *Chemical Geology: Isotope Geoscience section* **58,** 1–22 (1985).
20. Gleadow, A. J. W., Duddy, I. R., Green, P. F. & Lovering, J. F. Confined fission track lengths in apatite: a diagnostic tool for thermal history analysis. *Contr. Mineral. and Petrol.* **94,** 405–415 (1986).
21. Gleadow, A. J. W., Duddy, I. R., Green, P. F. & Hegarty, K. A. Fission track lengths in the apatite annealing zone and the interpretation of mixed ages. *Earth and Planetary Science Letters* **78,** 245–254 (1986).
22. Hurford, A. J. Standardization of fission track dating calibration: Recommendation by the Fission Track Working Group of the I.U.G.S. Subcommission on Geochronology. *Chemical Geology: Isotope Geoscience section* **80,** 171–178 (1990).
23. Brandon, M. T., Roden-Tice, M. K. & Garver, J. I. Late Cenozoic exhumation of the Cascadia accretionary wedge in the Olympic Mountains, northwest Washington State. *Geological Society of America Bulletin* **110,** 985–1009 (1998).
24. Fox, M., Herman, F., Willett, S. D. & May, D. A. A linear inversion method to infer exhumation rates in space and time from thermochronometric data. *Earth Surface Dynamics* **2,** 47–65 (2014).
25. Rahl, J. M., Ehlers, T. A. & van der Pluijm, B. A. Quantifying transient erosion of orogens with detrital thermochronology from syntectonic basin deposits. *Earth and Planetary Science Letters* **256,** 147–161 (2007).
26. Whipp, D. M., Ehlers, T. A., Braun, J. & Spath, C. D. Effects of exhumation kinematics and topographic evolution on detrital thermochronometer data. *J. Geophys. Res.* **114,** F04021 (2009).
27. Finlayson, D. P., Montgomery, D. R. & Hallet, B. Spatial coincidence of rapid inferred erosion with young metamorphic massifs in the Himalayas. *Geology* **30,** 219–222 (2002).
28. Bermúdez, M. A., Beek, P. A. van der & Bernet, M. Strong tectonic and weak climatic control on exhumation rates in the Venezuelan Andes. *Lithosphere* **5,** 3–16 (2013).
29. Wilson, J. P. & Gallant, J. C. *Terrain Analysis: Principles and Applications*. (Wiley, 2000).
30. Wobus, C. *et al.* Tectonics from topography: Procedures, promise, and pitfalls. *Geological Society of America Special Papers* **398,** 55–74 (2006).
31. Bizzi, S. & Lerner, D. N. The Use of Stream Power as an Indicator of Channel Sensitivity to Erosion and Deposition Processes. *River Res. Applic.* **31,** 16–27 (2015).
32. Anderson, R. S. & Anderson, S. P. *Geomorphology: The mechanics and chemistry of landscapes*. (Cambridge Univ Press, 2010).
33. Tucker, G. E. & Whipple, K. X. Topographic outcomes predicted by stream erosion models: Sensitivity analysis and intermodel comparison. *J. Geophys. Res.* **107,** 2179 (2002).
34. New, M., Hulme, M. & Jones, P. Representing Twentieth-Century Space–Time Climate Variability. Part II: Development of 1901–96 Monthly Grids of Terrestrial Surface Climate. *J. Climate* **13,** 2217–2238 (2000).

35. Bookhagen, B. High resolution spatiotemporal distribution of rainfall seasonality and extreme events based on a 12-year TRMM time serie. (2013).
36. Hengl, T. *et al.* SoilGrids1km — Global Soil Information Based on Automated Mapping. *PLoS ONE* **9,** e105992 (2014).
37. *World reference base for soil resources, 2006: a framework for international classification, correlation, and communication*. (Food and Agriculture Organization of the United Nations, 2006).
38. Crawley, M. J. *The R book*. (John Wiley & Sons Ltd, 2007).
39. Burnham, K. P. & Anderson, D. R. *Model Selection and Multimodel Inference - A Practical Information - Theoretic Approach*. (Springer-Verlag, 2002).
40. Legendre, P. & Legendre, L. *Numerical Ecology*. (Elsevier, 1998).
41. Kissling, W. D. & Carl, G. Spatial Autocorrelation and the Selection of Simultaneous Autoregressive Models. *Global Ecology and Biogeography* **17,** 59–71 (2008).
42. Rahbek, C. & Graves, G. R. Multiscale assessment of patterns of avian species richness. *PNAS* **98,** 4534–4539 (2001).
43. Jetz, W. & Rahbek, C. Geometric constraints explain much of the species richness pattern in African birds. *Proceedings of the National Academy of Sciences* **98,** 5661–5666 (2001).
44. Colwell, R. K., Rahbek, C. & Gotelli, N. J. The Mid-Domain Effect and Species Richness Patterns: What Have We Learned So Far? *The American Naturalist* **163,** E1–E23 (2004).
45. Rahbek, C. *et al.* Predicting continental-scale patterns of bird species richness with spatially explicit models. *Proceedings of the Royal Society of London B: Biological Sciences* **274,** 165–174 (2007).

SUPPLEMENTARY INFORMATION

I. Mountain regions surveyed

Below we provide a brief and introductory characterisation of the mountain regions considered for this study (Fig. 1 and Fig. 3), including key references on their orogeny, configuration, and abiotic and biotic settings. The length of these descriptions varies due to differences in the available literature. Similarly, only four regions (North America, the Andes, Eastern Africa, and High Asia) had enough available data to allow statistical analyses of species richness in relation to climate and geology.

North America
Mountain ranges in North America show a strong longitudinal gradient in relief, with a mountainous western region (North American Cordillera; the focus of our analysis) that has been tectonically active since the Cretaceous, mainly through strike slip on the San Andreas and extension in the Basin and Range province, with major changes to the landscape over the last 40 Myr[1]. The extensive eastern region (Appalachians; not included in our analyses) comprises the craton and the eroded remnants of Palaeozoic orogenies. The Rockies and Front Range in Colorado are currently inactive. The Rockies in Canada show some convergence[2]. Steep bioclimatic gradients between desert basins and rugged mountain ranges characterise the montane and intermontane regions. Coastal ranges along the Pacific capture high levels of precipitation year-round and support some of the highest-biomass forests in the world[3].

Europe
High topographic complexity characterises much of southern Europe and adjacent Anatolia, as well as western Scandinavia. The major mountain belt—including the Alps, Carpathians, and associated ranges north of the Mediterranean Sea— resulted from orogenies in the late Mesozoic and middle to late Cenozoic[4] and run east-west, serving as orographic and dispersal barriers. Mountain vertebrate richness in Europe peaks in the Pyrenees, the western Alps, and the Balkans, and is lowest in Scandinavia.

High Asia
The Central Asian Highlands (hereafter 'High Asia') extend over 4000 km and comprise the Qinghai-Tibetan Plateau and the Tianshan, Hindu-Kush, Himalayan and Hengduanshan mountain regions. Climate in this region has been mainly driven by the interactions among mountain and plateau formation and atmospheric circulation patterns. The topographic history of High Asia has been intensely studied [5,6, 7, 8] and the key geological events are the Indo-Eurasian collision (ca. 55–40 Myr ago) and uplift of the Himalayas (ca. 20–15 Myr ago) [9,10]. Hengduanshan might have a younger uplift history, mainly in the Pliocene[11]. These events contributed to strengthen the Asian monsoon system (distinct wet/dry seasonality) in the Miocene[12, 13], although a resilient system of monsoonal circulations existed at least since the Eocene. The onset of the monsoons was modulated by a combination of various factors, including Himalayan and Tibetan surface uplift, and possibly also the retreat of the Tarim Sea[14], changes in global atmospheric pCO_2 [15] and global climate shifts including the Eocene-Oligocene transition [16] or general global cooling [17]. Further evidence for these events

derive from fossil flora [18, 19, 20], windblown dust provenance, oxygen isotope-based palaeoclimate records, and climatic simulations [21, 15, 22]. The Qinghai-Tibetan Plateau forms a barrier to subtropical tropospheric airflow and pulls the Intertropical Convergence Zone seasonally far north of the equator [23], affecting the global distribution of heat and moisture [18,23], yet it seems to have limited influence on central Asian moisture transport through westerly winds [24].

Australia

Australia as a low-lying continent has three key regions of elevated topography: the Carnarvon Range in the northwest, the Macdonnell ranges in the centre of the continent, and the Great Dividing Range, or Eastern Highlands, paralleling the eastern coast. Although Australian mountains are not high (the highest peak is Mt Kosciuszko at 2230 m), they range into alpine habitats, and at least in Queensland, have a marked impact on the local climate. Mountain precipitation exhibits large variation: the central and western mountains are very dry, compared to the mesic climate of the Great Dividing Range in the east. The southern portion of the Great Dividing Range was locally glaciated during the colder phases of the Pleistocene, and the region is still associated with periglacial environments and high lake stands [25] and has frosty winters. Highest vertebrate diversity in Australian mountains occurs in the Great Dividing Range. Plant diversity patterns [26] broadly mirror those of vertebrates (Fig. 1), with the highest species richness associated with the central portion of the Great Dividing Range near New England.

Eastern Africa

The geological and climatic history of eastern Africa is in stark contrast to that in southern Africa. In eastern Africa (Supplementary Fig. 8), much of the topography and mountain building reflects the development of the East African Rift system (Western and Eastern Rift) during the Miocene [27]. The mountains in this region are consequently much younger than the southern African mountains, and major mountain ranges, such as the Rwenzori, date only from the Pliocene [28].

Southern Africa

Southern Africa (Supplementary Fig. 7) is dominated by a central plateau (1000–2000 m), with the highest peaks reaching 3000 m. The plateau is separated by an abrupt escarpment from a narrow coastal plain, which both have been in place throughout the Cenozoic and probably since the continental breakup in the Jurassic [29]. At the separation of Africa from Gondwana in the late Jurassic, the escarpment was on the continental margins, and rapid erosion during the Cretaceous resulted in the retreat of the escarpment to its present position, with apparently little further retreat during the Cenozoic [30]. During this process, the Cape Fold Mountains were exhumed. These are composed of a resistant quarzitic sandstone, and have probably retained their steep slopes and craggy peaks throughout the Cenozoic [31]. The eastern half of the subcontinent, centred around the Drakensberg, was however uplifted by up to 900 m during the Pliocene, increasing its topography [29]. The eastern escarpment and coastal plain are today much wetter than the western escarpment and coastal plain, and an east-west aridity gradient extends across the central plateau [32]. The distribution of vertebrate diversity follows the west-east gradient of increasing precipitation and a southeast to northwest gradient of increasing temperature. The gradual aridification of the western half of the subcontinent since the middle Miocene [33, 34] has led to the

establishment of a summer-dry and winter-wet climate at the southwestern tip of the continent [35]. The huge plant diversity of southern Africa [36], especially the Cape flora which contains an extreme level of endemism, has been linked to this Mediterranean-type climate, topographic barriers (resistant sandstones), and long-term geological and climatic stability [37, 38]. The low vertebrate diversity in the southwestern part of the subcontinent, from southern Namibia to Port Elizabeth (the winter-rainfall region), could be caused by the dominant sclerophyllous vegetation.

Eastern South America

The mountains of eastern South America are generally older and lower than the Andes, ending their orogeny around 18–15 Myr ago [39] and reaching today less than half the elevation of the highest Andean mountains (ca. 2,900 m vs. ca. 7,000 m). There is a precipitation gradient from the coast to inland reflected by a transition in ecosystems, from the Atlantic rain forest with dense tropical vegetation on the eastern mountain slopes, replaced by open savanna vegetation (the Cerrado) on the Brazilian plateau (ca. 600–800 m), and shrublands in the semi-arid Caatinga of northeastern Brazil. The Caatinga, Cerrado, Chaco and Pantanal form together a diagonal belt of seasonally dry vegetation that act as a biogeographical barrier for mountain and rain forest organisms. Vertebrate diversity has not only been linked to current climate but also to the effect of vegetation stability, in particular refugia, through Quaternary climatic cycles [40]. Mountain vertebrate diversity peaks in southeastern Brazil, following a reverse latitudinal diversity gradient previously reported for birds [41].

The Andes

The Andes reached about half of their current elevation in the middle to late Miocene[42]. This uplift resulted in an orographic barrier that greatly modified South American climate [43,44,45]. The temperature gradient is strongly influenced by the latitudinal south-north orientation of the mountain range and by different climate modes originating in the Pacific and the Atlantic [46]. In the north, this barrier, enhanced by its concave shape, captures the humid air masses of the Intertropical Convergence Zone and funnels them back into the Amazon basin as precipitation [47,48], which is further driven and maintained by forest cover [49] or reroutes air masses to the higher latitudes. The three Andean subregions (northern, central and southern) differ in their genesis [50] and the way in which they interact with atmospheric circulation, resulting in a wide range of environmental conditions. Uplift of the northern Andes peaked in the late Neogene c. 12–4 Myr ago and is linked to the Neogene collision of the South American and Caribbean plates with the Panama Arch [51, 52, 53], which resulted in their characteristic trifurcate pattern. Neogene sedimentary records provide evidence of a change from high precipitation to arid conditions around 9 Myr ago, which is linked to the changing pattern of the South American low-level jet [54, 43,55]. This process redefined landscape and biodiversity patterns in the Andes and Amazonia and shaped the basic geographic conditions of today[56]. A large portion of the Central Andes, in particular its extensive high-elevation Plateau (the Altiplano), uplifted rapidly and extensively during two distinct phases, between 30-25 Ma and, more notably, between 10-5 Ma [42]. In contrast, the orographic history of the Southern Andes has been less summarised by recent reviews.

II. Supplementary tables and figures

Supplementary Table S1: Predictor variables used for analysing vertebrate species richness across the world's mountains.

Abbreviation	Description	Unit	Source
PREC	Annual precipitation (BIO12)	mm yr^{-1}	Worldclim (version 1.4)[57]
TEMP	Mean annual temperature (BIO1)	°C × 10	Worldclim (version 1.4) [57]
TEMP RANGE	Temperature annual range (maximum temperature of warmest month minus minimum temperature of coldest month; BIO7 = BIO5-BIO6)	°C × 10	Worldclim (version 1.4) [57]
PREC SEASON	Precipitation seasonality (coefficient of variation of monthly values; BIO15)	mm	Worldclim (version 1.4) [57]
RELIEF	Topographic relief measured as range in elevation (maximum minus minimum elevation)	m	Calculated for this analysis using the SRTM 90 m database (version 4.1)[58]
COOL AGE	Cooling age (mean value of apatite fission-track ages per grid cell)	Myr	Calculated from different apatite fission-track datasets [59,56,60,61,62,63,64,65]
LONG EROSION	Long-term erosion measured as cooling rate, derived from apatite fission-track values. For more details see text and Figure S1.	km Myr^{-1}	Calculated using the approach described by Fox et al (2014)[66] and Herman et al. (2013)[59], which is based on a formal inversion of thermochronological dataset.
SHORT EROSION	Short-term erosion rate measured as the total stream power (TSP) index weighted with precipitation data, i.e. rate of energy loss to channel bed per unit length (energy per unit time), calculated as $TSP_P = \sum (A_P P) S$, where A_P is upstream drainage area (used as a proxy of discharge) for each pixel, P is the average precipitation from 1961 to 1990, and 1997 to 2009; and S is local slope. The summation sign implies summing along the flow-lines in order to calculate the flow accumulation.	Wm^{-1}	Calculated for this analysis using the SRTM 90 m database (version 4.1)[58]. Precipitation data was obtained for period 1961 to 1990, and 1997 to 2009 ([67,68])
SOIL	Number of soil types	count	SoilGrids1km[69]

Supplementary Table S2: Sources for the regional derivation of parameters to estimate apatite fission tracks.

Region	Areas	References for parameters
North America	Colorado, Appalachians, Sierra Nevada	[70] [71] [72]
Europe	Alps	[73] [74]
High Asia	Himalayas	[75] [76]
Australia		[77]
The Andes	Venezuelan Andes, Central Cordillera	[78]
Eastern South America	Altiplano Plateau	[79]
Southern Africa	Congo Basin, Namibia, Zambia	[80]
Eastern Africa		[81]

Supplementary Table S3: Characteristics of the global mountain dataset in relation to variation in vertebrate species richness, climate, and geology. The dataset covered a total of 327 grid cells with global extent (Fig. 3 in main text) and a spatial resolution of 1º × 1º. For abbreviation and units of predictor variables see Supplementary Table S1.

Variable	Minimum	Median	Mean	Maximum
Vertebrate species richness	25	255	327	1135
PREC	8	648	719	2581
TEMP	-65	98	102	259
TEMP RANGE	104	274	281	476
PREC SEASON	10	68	69	177
RELIEF	114	2736	2930	7537
COOL AGE	0.5	51	84	368
LONG EROSION	0.01	0.11	0.28	4.99
SHORT EROSION	340	234000	2862000	101200000
SOIL	3	12	12	22

Supplementary Table S4: Results from global multi-predictor regression models to explain vertebrate species richness across the world's mountains. Two types of models are compared, a non-spatial ordinary least square (OLS) regression and a spatial simultaneous autoregressive (SAR) model. The response variable (vertebrate species richness) as well as short-term and long-term erosion variables were log-transformed. All variables were scaled to a mean of zero and variance of 1 before the analysis to make model coefficients comparable. Standardised coefficients, the explained variance of the environmental components (R^2_{PRED}), the explained variance of the full SAR model including both environment and space (R^2_{FULL}), the Moran's *I*, and the *p*-value of Moran's *I* are given. Significance of Moran's *I* was determined by permutation tests (n = 999 permutations). Significance levels: ***p < 0.001; **p < 0.01; *p < 0.05. n.s., not significant. Abbreviations and explanations of predictor variables are found in Table 1 and Supplementary Table S1.

	OLS		SAR	
	Coefficient	*p*	Coefficient	*p*
Intercept	0.217	***	0.121	n.s.
PREC	0.455	***	0.506	***
$PREC^2$	-0.091	**	-0.126	***
TEMP	0.392	***	0.211	***
TEMP RANGE	-		-	-
PREC SEASON	-		-	-
RELIEF	0.259	***	0.123	**
COOL AGE	0.178	*	0.120	*
$COOL\ AGE^2$	-0.126	***	-0.039	n.s.
LONG EROSION	-		-	
SHORT EROSION	0.135	*	0.041	n.s.
SOIL	0.121	*	0.120	**
R^2_{PRED}	0.53		0.49	
R^2_{FULL}	-		0.84	
Moran's *I*	0.631	***	-0.006	n.s.

Supplementary Table S5: Results from regional multi-predictor regression models to explain vertebrate species richness in the mountains of Northern America, the Andes, Eastern Africa, and High Asia. Two types of models are compared (except for North America for which no residual spatial autocorrelation was detected), a non-spatial ordinary least square (OLS) regression and a spatial simultaneous autoregressive (SAR) model. The response variable (vertebrate species richness) as well as short-term and long-term erosion variables were log-transformed. All variables were scaled to a mean of zero and variance of 1 before the analysis to make model coefficients comparable. Standardised coefficients, the explained variance of the environmental components (R^2_{PRED}), the explained variance of the full SAR model including both environment and space (R^2_{FULL}), the Moran's *I*, and the *p*-value of Moran's *I* are given. Significance of Moran's *I* was determined by permutation tests (n = 999 permutations). Significance levels: ***$p < 0.001$; **$p < 0.01$; *$p < 0.05$. n.s., not significant. Abbreviations and explanations of predictor variables are found in Table 1 and Supplementary Table S1.

	North America		The Andes		Eastern Africa		High Asia	
	OLS	SAR	OLS	SAR	OLS	SAR	OLS	SAR
Intercept	0.273*	-	0.201$^{n.s.}$	0.367$^{n.s.}$	0.410***	0.422**	0.195**	0.018$^{n.s.}$
PREC	0.759**	-	0.781***	1.149***	0.447***	0.491***	0.408***	0.350***
PREC^2	-0.282**	-	-0.204*	-0.360***	-0.423***	-0.418***	-0.197***	-0.100*
TEMP	-	-	0.371***	0.120$^{n.s.}$	-	-	0.233**	0.061$^{n.s.}$
TEMP RANGE	1.185***	-	-	-	-	-	-0.277*	-0.339**
PREC SEASON	0.453***	-	0.305*	0.450***	-0.302**	-0.327***	-	-
RELIEF	0.256$^{n.s.}$	-	0.218**	0.047$^{n.s.}$	-	-	0.162*	0.150**
COOL AGE	-	-	-	-	-0.290*	-0.266***	0.257**	0.073$^{n.s.}$
LONG EROSION	-0.319**	-	-	-	-0.293*	-0.308**	0.257*	0.152**
SHORT EROSION	-	-	0.196*	0.179*	-	-	0.127*	-0.000$^{n.s.}$
SOIL	0.337*	-	-	-	0.284**	0.232**	0.073$^{n.s.}$	-0.019$^{n.s.}$
R^2_{PRED}	0.79	-	0.78	0.70	0.90	0.89	0.81	0.76
R^2_{FULL}	-	-	-	0.90	-	0.93	-	0.94
Moran's *I*	0.01$^{n.s.}$	-	0.40***	-0.01$^{n.s.}$	0.29*	0.15$^{n.s.}$	0.49***	0.019$^{n.s.}$

North America

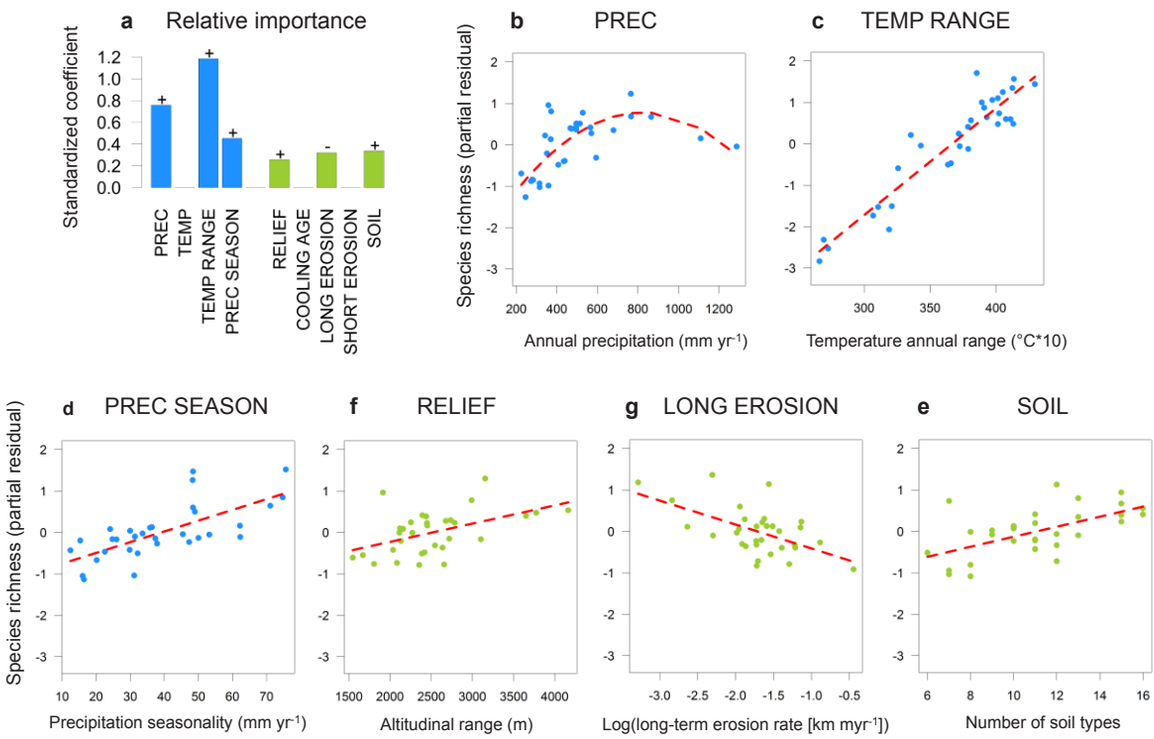

Supplementary Fig S1. Determinants of vertebrate species richness for North America. a, Relative importance (standardised coefficients) of predictor variables from the regional multi-predictor model across 1° grid cells, relating species richness of vertebrates to climatic (blue) and geological (green) predictor variables (the direction of effect is indicated as + or -). **b–e** Partial residual plots of predictor variables from the same model. Partial residuals represent the relationship between a response and a predictor variable when all other predictor variables in the model are statistically controlled. Predictor variables are explained in Table S1.

Andes

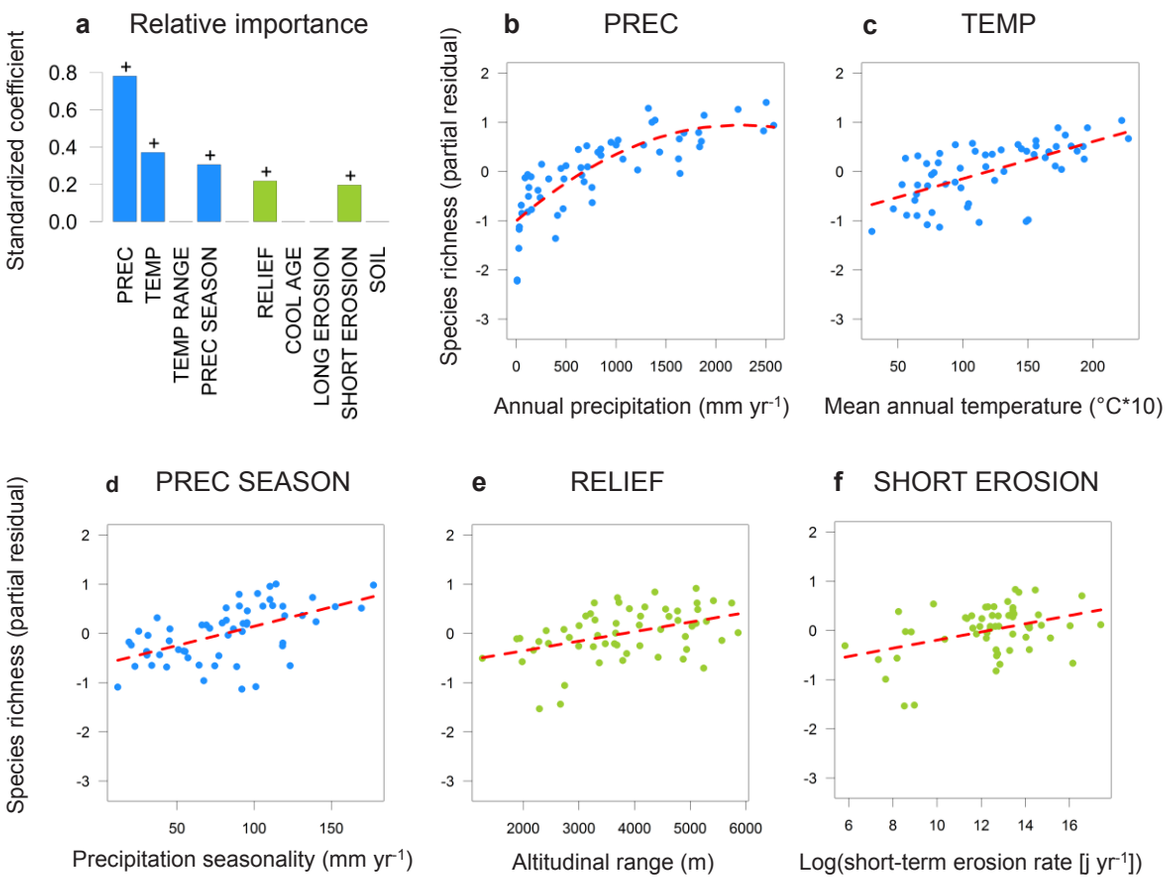

Supplementary Fig S2. Determinants of vertebrate species richness for the Andes. a, Relative importance (standardised coefficients) of predictor variables from the regional multi-predictor model across 1° grid cells, relating species richness of vertebrates to climatic (blue) and geological (green) predictor variables (the direction of effect is indicated as + or -). **b–f** Partial residual plots of predictor variables from the same model. Partial residuals represent the relationship between a response and a predictor variable when all other predictor variables in the model are statistically controlled. Predictor variables are explained in Table S1.

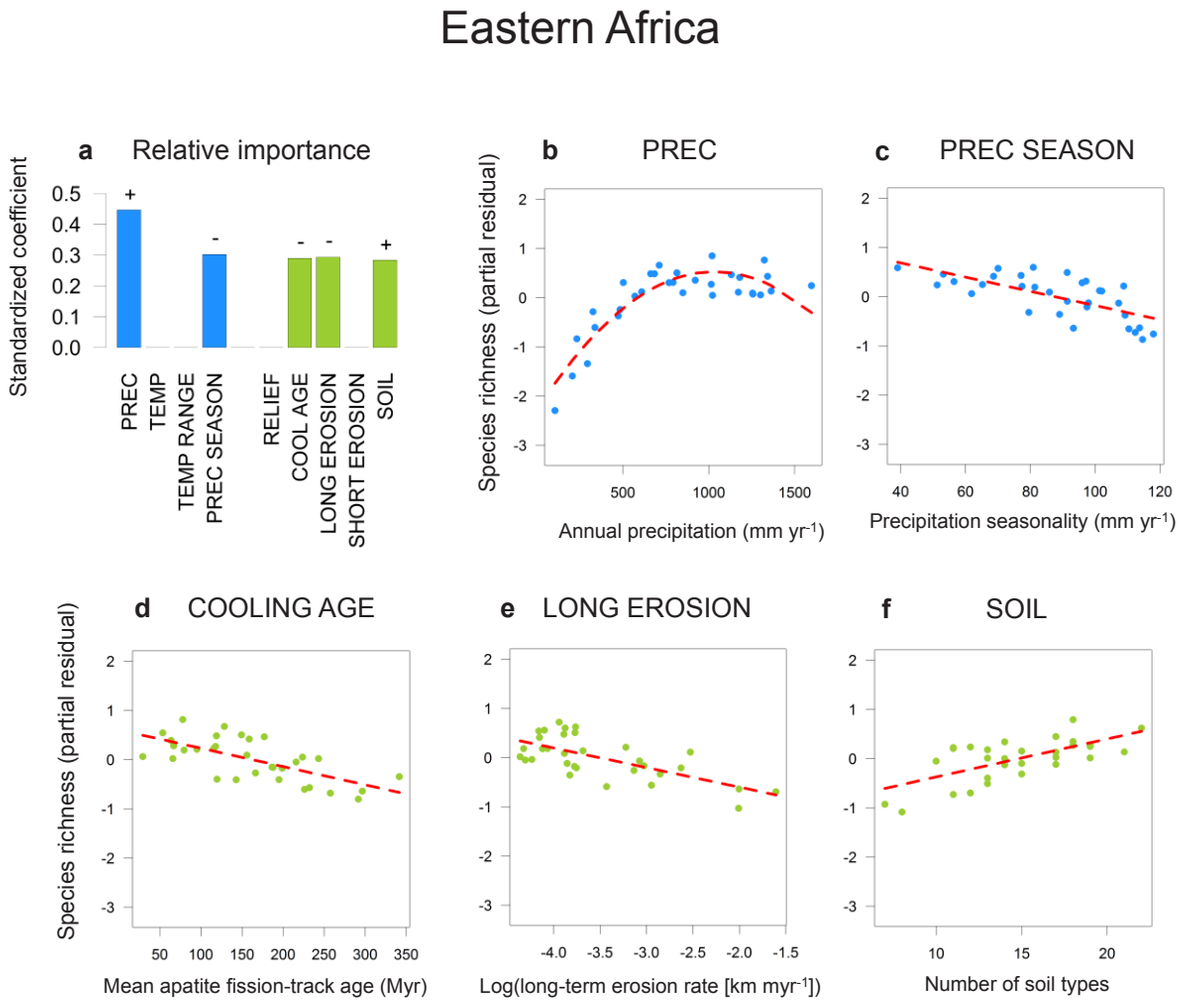

Supplementary Fig S3. Determinants of vertebrate species richness for Eastern Africa. a, Relative importance (standardised coefficients) of predictor variables from the regional multi-predictor model across 1° grid cells, relating species richness of vertebrates to climatic (blue) and geological (green) predictor variables (the direction of effect is indicated as + or -). **b–f** Partial residual plots of predictor variables from the same model. Partial residuals represent the relationship between a response and a predictor variable when all other predictor variables in the model are statistically controlled. Predictor variables are explained in Table S1.

High Asia

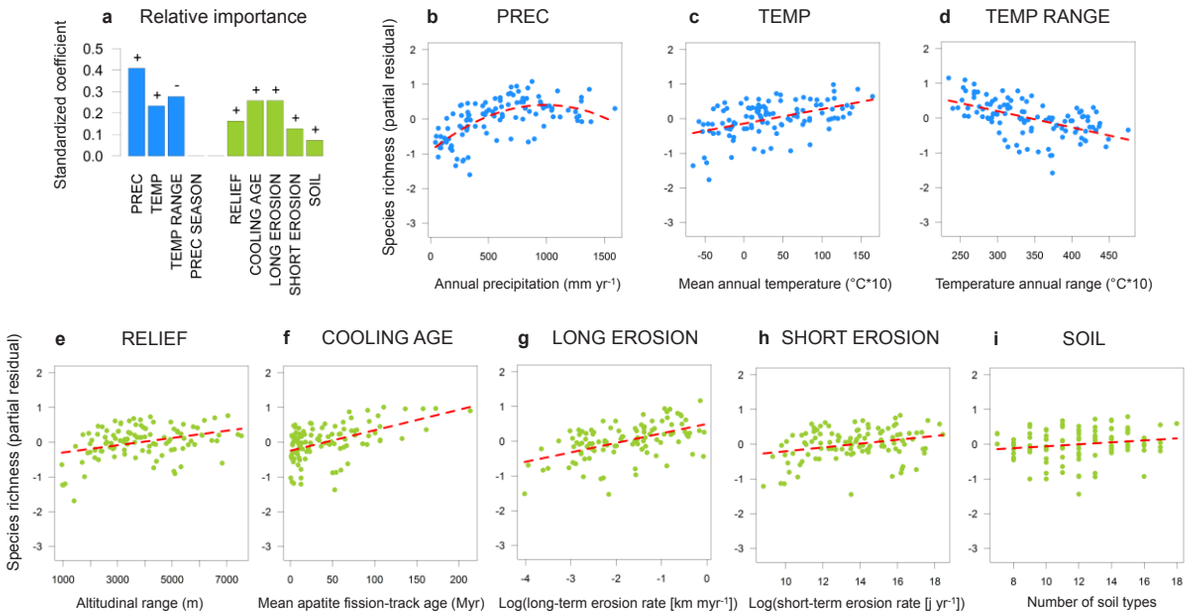

Supplementary Fig S4. Determinants of vertebrate species richness for High Asia. a, Relative importance (standardised coefficients) of predictor variables from the regional multi-predictor model across 1° grid cells, relating species richness of vertebrates to climatic (blue) and geological (green) predictor variables (the direction of effect is indicated as + or -). **b–i** Partial residual plots of predictor variables from the same model. Partial residuals represent the relationship between a response and a predictor variable when all other predictor variables in the model are statistically controlled. Predictor variables are explained in Table S1.

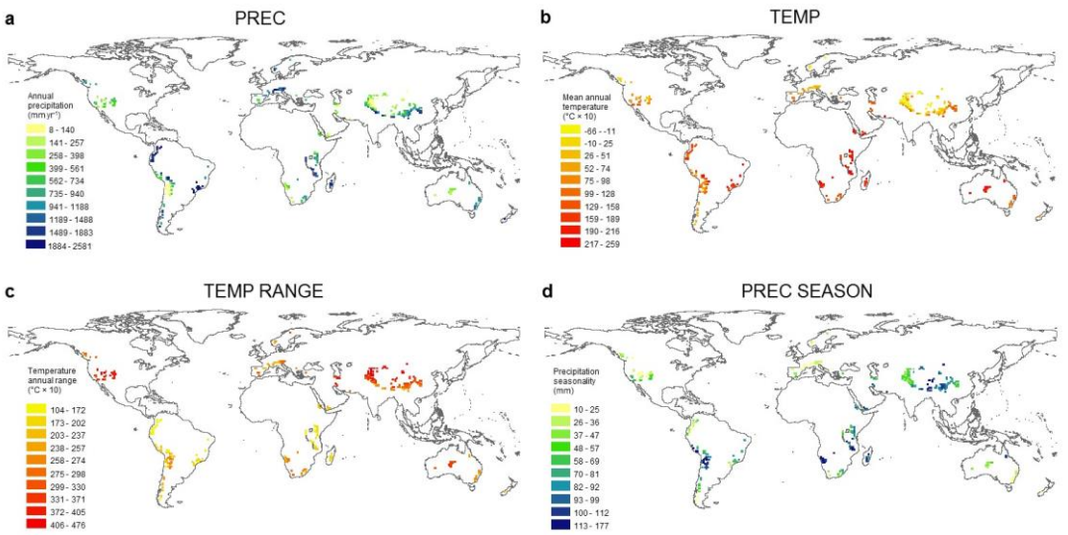

Supplementary Figure S5. Climatic predictor variables and their global variation across all included 1° grid cells (n = 327). Maps are plotted with quantile classification and a World Geodetic System projection (WGS 1984). See Table S1 for details on predictor variables.

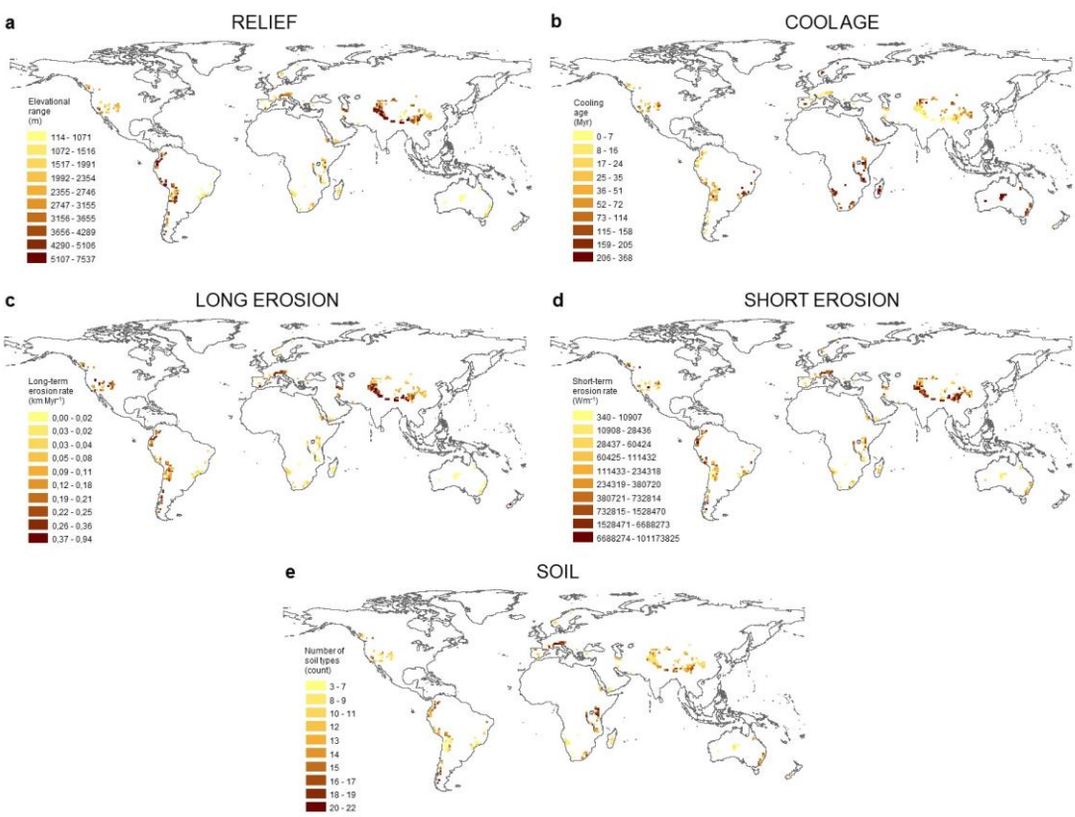

Supplementary Figure S6. Geological predictor variables and their global variation across all included 1° grid cells (n = 327). Maps are plotted with quantile classification and a World Geodetic System projection (WGS 1984). See Table S1 for details on predictor variables.

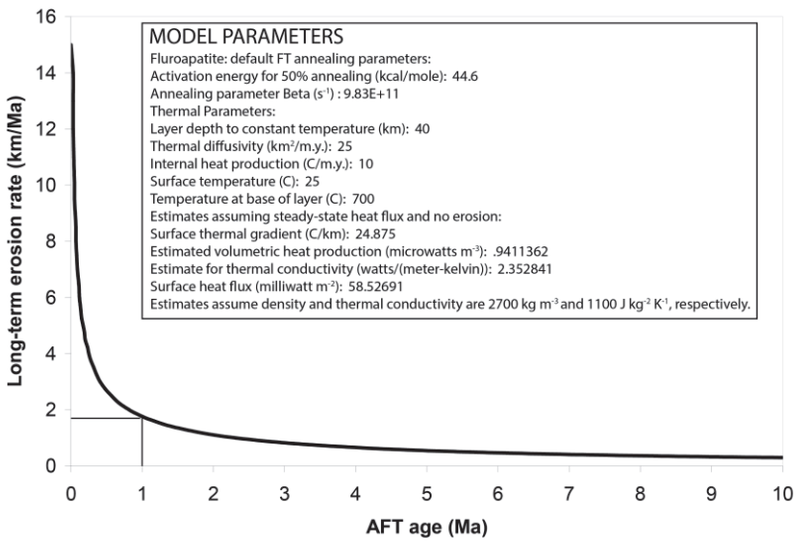

Supplementary Figure S7. Hypothetical age-cooling rate relationships plots derived from age2edot. Model parameters are defined in the box. Given the cooling rate $\dot{\varepsilon}$ and the temperature with respect to depth, we can use the Dodson equation25 to solve for Tc, and for the depth of closure zc. The predicted cooling age is given by $\frac{z_c}{\dot{\varepsilon}}$. In practical terms, the predicted cooling age is given for each apatite fission-track (AFT) age. Hence, it is possible to calculate the long-term erosion rate as: $\dot{\varepsilon} = \frac{z_c}{AFTage}$

III. Supplementary references

1. Dickinson, W. R. Evolution of the North American Cordillera. *Annual Review of Earth and Planetary Sciences* **32,** 13–45 (2004).
2. Champagnac, J.-D., Molnar, P., Sue, C. & Herman, F. Tectonics, climate, and mountain topography. *J. Geophys. Res.* **117,** B02403 (2012).
3. Keith, H., Mackey, B. G. & Lindenmayer, D. B. Re-evaluation of forest biomass carbon stocks and lessons from the world's most carbon-dense forests. *PNAS* **106,** 11635–11640 (2009).
4. Schmid, S. M., Fügenschuh, B., Kissling, E. & Schuster, R. Tectonic map and overall architecture of the Alpine orogen. *Eclogae geol. Helv.* **97,** 93–117 (2004).
5. Mulch, A. & Chamberlain, C. P. Earth science: The rise and growth of Tibet. *Nature* **439,** 670–671 (2006).
6. Rowley, D. B. & Currie, B. S. Palaeo-altimetry of the late Eocene to Miocene Lunpola basin, central Tibet. *Nature* **439,** 677–681 (2006).
7. Saylor, J. E. *et al.* The late Miocene through present paleoelevation history of southwestern Tibet. *Am J Sci* **309,** 1–42 (2009).
8. Ding, L. *et al.* The Andean-type Gangdese Mountains: Paleoelevation record from the Paleocene–Eocene Linzhou Basin. *Earth and Planetary Science Letters* **392,** 250–264 (2014).
9. Yin, A. & Harrison, T. M. Geologic Evolution of the Himalayan-Tibetan Orogen. *Annual Review of Earth and Planetary Sciences* **28,** 211–280 (2000).
10. Gébelin, A. *et al.* The Miocene elevation of Mount Everest. *Geology* G34331.1 (2013). doi:10.1130/G34331.1
11. Sun, B.-N. *et al.* Reconstructing Neogene vegetation and climates to infer tectonic uplift in western Yunnan, China. *Palaeogeography, Palaeoclimatology, Palaeoecology* **304,** 328–336 (2011).
12. Sun, X. & Wang, P. How old is the Asian monsoon system?—Palaeobotanical records from China. *Palaeogeography, Palaeoclimatology, Palaeoecology* **222,** 181–222 (2005).
13. Guo, Z. T. *et al.* A major reorganization of Asian climate by the early Miocene. *Clim. Past* **4,** 153–174 (2008).
14. Bosboom, R. *et al.* Linking Tarim Basin sea retreat (west China) and Asian aridification in the late Eocene. *Basin Res* **26,** 621–640 (2014).
15. Licht, A. *et al.* Asian monsoons in a late Eocene greenhouse world. *Nature* **513,** 501–506 (2014).
16. Dupont-Nivet, G. *et al.* Tibetan plateau aridification linked to global cooling at the Eocene–Oligocene transition. *Nature* **445,** 635–638 (2007).
17. Jiang, H. & Ding, Z. A 20 Ma pollen record of East-Asian summer monsoon evolution from Guyuan, Ningxia, China. *Palaeogeography, Palaeoclimatology, Palaeoecology* **265,** 30–38 (2008).
18. Molnar, P., Boos, W. R. & Battisti, D. S. Orographic Controls on Climate and Paleoclimate of Asia: Thermal and Mechanical Roles for the Tibetan Plateau. *Annual Review of Earth and Planetary Sciences* **38,** 77–102 (2010).
19. Quan, C., Liu, Y.-S. (Christopher) & Utescher, T. Eocene monsoon prevalence over China: A paleobotanical perspective. *Palaeogeography, Palaeoclimatology, Palaeoecology* **365–366,** 302–311 (2012).
20. Shukla, A., Mehrotra, R. C., Spicer, R. A., Spicer, T. E. V. & Kumar, M. Cool equatorial terrestrial temperatures and the South Asian monsoon in the Early Eocene: Evidence from the Gurha Mine, Rajasthan, India. *Palaeogeography, Palaeoclimatology, Palaeoecology* **412,** 187–198 (2014).
21. Huber, M. & Goldner, A. Eocene monsoons. *Journal of Asian Earth Sciences* **44,** 3–23 (2012).
22. Licht, A. *et al.* Resilience of the Asian atmospheric circulation shown by Paleogene dust provenance. *Nature Communications* **7,** 12390 (2016).

23. Lippert, P. C., Hinsbergen, D. J. J. van & Dupont-Nivet, G. Early Cretaceous to present latitude of the central proto-Tibetan Plateau: A paleomagnetic synthesis with implications for Cenozoic tectonics, paleogeography, and climate of Asia. *Geological Society of America Special Papers* **507,** SPE507-01 (2014).
24. Caves, J. K. *et al.* Role of the westerlies in Central Asia climate over the Cenozoic. *Earth and Planetary Science Letters* **428,** 33–43 (2015).
25. Barrows, T. T., Stone, J. O., Fifield, L. K. & Cresswell, R. G. Late Pleistocene Glaciation of the Kosciuszko Massif, Snowy Mountains, Australia. *Quaternary Research* **55,** 179–189 (2001).
26. Crisp, M. D., Laffan, S., Linder, H. P. & Monro, A. Endemism in the Australian flora. *Journal of Biogeography* **28,** 183–198 (2001).
27. Moucha, R. & Forte, A. M. Changes in African topography driven by mantle convection. *Nature Geoscience* **4,** 707–712 (2011).
28. Kaufmann, G. & Romanov, D. Landscape evolution and glaciation of the Rwenzori Mountains, Uganda: Insights from numerical modeling. *Geomorphology* **138,** 263–275 (2012).
29. Partridge, T. C. & Maud, R. R. in *Macro-scale geomorphic evolution of southern Africa* (eds. Partridge, T. C. & Maud, R. R.) 3–18 (Oxford University Press, 2000).
30. Tinker, J., de Wit, M. & Brown, R. Mesozoic exhumation of the southern Cape, South Africa, quantified using apatite fission track thermochronology. *Tectonophysics* **455,** 77–93 (2008).
31. Scharf, T. E., Codilean, A. T., Wit, M. de, Jansen, J. D. & Kubik, P. W. Strong rocks sustain ancient postorogenic topography in southern Africa. *Geology* **41,** 331–334 (2013).
32. Tyson, P. & Partridge, T. C. in *The Cenozoic of Southern Africa* (eds. Partridge, T. C. & Maud, R. R.) 371–387 (Oxford University Press, 2000).
33. Dupont, L. M., Rommerskirchen, F., Mollenhauer, G. & Schefuß, E. Miocene to Pliocene changes in South African hydrology and vegetation in relation to the expansion of C4 plants. *Earth and Planetary Science Letters* **375,** 408–417 (2013).
34. Hoetzel, S., Dupont, L., Schefuß, E., Rommerskirchen, F. & Wefer, G. The role of fire in Miocene to Pliocene C4 grassland and ecosystem evolution. *Nature Geosci* **6,** 1027–1030 (2013).
35. Dupont, L. M., Linder, H. P., Rommerskirchen, F. & Schefuß, E. Climate-driven rampant speciation of the Cape flora. *Journal of Biogeography* **38,** 1059–1068 (2011).
36. Linder, H. P. Plant diversity and endemism in sub-Saharan tropical Africa. *Journal of Biogeography* **28,** 169–182 (2001).
37. Schnitzler, J. *et al.* Causes of Plant Diversification in the Cape Biodiversity Hotspot of South Africa. *Syst Biol* **60,** 343–357 (2011).
38. Linder, H. P., Rabosky, D. L., Antonelli, A., Wüest, R. O. & Ohlemüller, R. Disentangling the influence of climatic and geological changes on species radiations. *J. Biogeogr.* **41,** 1313–1325 (2014).
39. Japsen, P. *et al.* Episodic burial and exhumation in NE Brazil after opening of the South Atlantic. *Geological Society of America Bulletin* B30515.1 (2012). doi:10.1130/B30515.1
40. Carnaval, A. C., Hickerson, M. J., Haddad, C. F. B., Rodrigues, M. T. & Moritz, C. Stability Predicts Genetic Diversity in the Brazilian Atlantic Forest Hotspot. *Science* **323,** 785–789 (2009).
41. Chaves, A. V., Freitas, G. H. S., Vasconcelos, M. F. & Santos, F. R. Biogeographic patterns, origin and speciation of the endemic birds from eastern Brazilian mountaintops: a review. *Systematics and Biodiversity* **13,** 1–16 (2015).
42. Garzione, C. N. *et al.* Rise of the Andes. *Science* **320,** 1304–1307 (2008).
43. Mulch, A., Uba, C. E., Strecker, M. R., Schoenberg, R. & Chamberlain, C. P. Late Miocene climate variability and surface elevation in the central Andes. *Earth and Planetary Science Letters* **290,** 173–182 (2010).

44. Poulsen, C. J., Ehlers, T. A. & Insel, N. Onset of Convective Rainfall During Gradual Late Miocene Rise of the Central Andes. *Science* **328,** 490–493 (2010).
45. Sepulchre, P., Sloan, L. C. & Fluteau, F. in *Amazonia: Landscape and Species Evolution* (eds. Hoorn, C. & Wesselingh, F. P.) 211–222 (Wiley-Blackwell Publishing Ltd., 2010).
46. Flantua, S. G. A. *et al.* Climate variability and human impact in South America during the last 2000 years: synthesis and perspectives from pollen records. *Climate of the Past* **12,** 483–523 (2016).
47. Garreaud, R. D., Vuille, M., Compagnucci, R. & Marengo, J. Present-day South American climate. *Palaeogeography, Palaeoclimatology, Palaeoecology* **281,** 180–195 (2009).
48. Barnes, J. B., Ehlers, T. A., Insel, N., McQuarrie, N. & Poulsen, C. J. Linking orography, climate, and exhumation across the central Andes. *Geology* **40,** 1135–1138 (2012).
49. Makarieva, A. M. & Gorshkov, V. G. Biotic pump of atmospheric moisture as driver of the hydrological cycle on land. *Hydrol. Earth Syst. Sci.* **11,** 1013–1033 (2007).
50. Elsen, P. R. & Tingley, M. W. Global mountain topography and the fate of montane species under climate change. *Nature Clim. Change* **advance online publication,** (2015).
51. Boschman, L. M., van Hinsbergen, D. J. J., Torsvik, T. H., Spakman, W. & Pindell, J. L. Kinematic reconstruction of the Caribbean region since the Early Jurassic. *Earth-Science Reviews* **138,** 102–136 (2014).
52. Bermúdez, M. A. *et al.* The detrital record of late-Miocene to Pliocene surface uplift and exhumation of the Venezuelan Andes in the Maracaibo and Barinas foreland basins. *Basin Res* **29,** 370–395 (2017).
53. Montes, C. *et al.* Middle Miocene closure of the Central American Seaway. *Science* **348,** 226–229 (2015).
54. Strecker, M. R. *et al.* Tectonics and Climate of the Southern Central Andes. *Annual Review of Earth and Planetary Sciences* **35,** 747–787 (2007).
55. Rohrmann, A. *et al.* Can stable isotopes ride out the storms? The role of convection for water isotopes in models, records, and paleoaltimetry studies in the central Andes. *Earth and Planetary Science Letters* **407,** 187–195 (2014).
56. Hoorn, C. *et al.* Amazonia Through Time: Andean Uplift, Climate Change, Landscape Evolution, and Biodiversity. *Science* **330,** 927–931 (2010).
57. Hijmans, R. J., Cameron, S. E., Parra, J. L., Jones, P. G. & Jarvis, A. Very high resolution interpolated climate surfaces for global land areas. *Int. J. Climatol.* **25,** 1965–1978 (2005).
58. Jarvis, A., Reuter, H. I., Nelson, A. & Guevara, E. SRTM 90m Digital Elevation Database v4.1 | CGIAR-CSI. (2008).
59. Herman, F. *et al.* Worldwide acceleration of mountain erosion under a cooling climate. *Nature* **504,** 423–426 (2013).
60. Dolati, A. Stratigraphy, structural geology and low-temperature thermochronology across the Makran accretionary wedge in Iran. (Eidgenössische Technische Hochschule ETH Z, 2010).
61. Rezaeian, M., Carter, A., Hovius, N. & Allen, M. B. Cenozoic exhumation history of the Alborz Mountains, Iran: New constraints from low-temperature chronometry. *Tectonics* **31,** TC2004 (2012).
62. Mbede, E. I. Tectonic development of the Rukwa rift basin in SW Tanzania. (FU Berlin, 1993).
63. Mbede, E. I. Tectonic setting and uplift analysis of the Pangani rift basin in northern Tanzania using apatite fission track thermochronology. *Tanzania Journal of Science* **27,** 23–38 (2001).
64. Biswal, T. K. & Seward, D. Tectonic implication of the Apatite Fission-track analysis of the mylonites from the Terrane Boundary Shear Zone of the Eastern Ghats Mobile Belt around Lakhna, Orissa. *Gondwana Research* **6,** 321–325 (2003).

65. Van der Beek, P., Mbede, E., Andriessen, P. & Delvaux, D. Denudation history of the Malawi and Rukwa Rift flanks (East African Rift System) from apatite fission track thermochronology. *Journal of African Earth Sciences* **26,** 363–385 (1998).
66. Fox, M., Herman, F., Willett, S. D. & May, D. A. A linear inversion method to infer exhumation rates in space and time from thermochronometric data. *Earth Surface Dynamics* **2,** 47–65 (2014).
67. New, M., Hulme, M. & Jones, P. Representing Twentieth-Century Space–Time Climate Variability. Part II: Development of 1901–96 Monthly Grids of Terrestrial Surface Climate. *J. Climate* **13,** 2217–2238 (2000).
68. Bookhagen, B. High resolution spatiotemporal distribution of rainfall seasonality and extreme events based on a 12-year TRMM time serie. (2013).
69. Hengl, T. *et al.* SoilGrids1km — Global Soil Information Based on Automated Mapping. *PLoS ONE* **9,** e105992 (2014).
70. Thomson, S. N. Late Cenozoic geomorphic and tectonic evolution of the Patagonian Andes between latitudes 42°S and 46°S: An appraisal based on fission-track results from the transpressional intra-arc Liquiñe-Ofqui fault zone. *Geological Society of America Bulletin* **114,** 1159–1173 (2002).
71. Densmore, M. S. Quantifying Long-Term Glacial Denudation with Low-Temperature Thermochronology. (2008).
72. McPhillips, D. & Brandon, M. T. Topographic evolution of the Sierra Nevada measured directly by inversion of low-temperature thermochronology. *Am J Sci* **312,** 90–116 (2012).
73. Bernet, M. Detrital Zircon Fission-Track Thermochronology of the Present-Day Isère River Drainage System in the Western Alps: No Evidence for Increasing Erosion Rates at 5 Ma. *Geosciences* **3,** 528–542 (2013).
74. Glotzbach, C., Bernet, M. & van der Beek, P. Detrital thermochronology records changing source areas and steady exhumation in the Western European Alps. *Geology* **39,** 239–242 (2011).
75. McQuarrie, N., Tobgay, T., Long, S. P., Reiners, P. W. & Cosca, M. A. Variable exhumation rates and variable displacement rates: Documenting recent slowing of Himalayan shortening in western Bhutan. *Earth and Planetary Science Letters* **386,** 161–174 (2014).
76. Patel, R. C. & Carter, A. Exhumation history of the Higher Himalayan Crystalline along Dhauliganga-Goriganga river valleys, NW India: New constraints from fission track analysis: EXHUMATION HISTORY OF KUMAON HIMALAYA. *Tectonics* **28,** n/a-n/a (2009).
77. O'Neill, C., Moresi, L., Lenardic, A. & Cooper, C. M. Inferences on Australia's heat flow and thermal structure from mantle convection modelling results. *Geological Society of America Special Papers* **372,** 169–184 (2003).
78. Bermúdez, M. A., Beek, P. A. van der & Bernet, M. Strong tectonic and weak climatic control on exhumation rates in the Venezuelan Andes. *Lithosphere* **5,** 3–16 (2013).
79. Schildgen, T. F., Hodges, K. V., Whipple, K. X., Reiners, P. W. & Pringle, M. S. Uplift of the western margin of the Andean plateau revealed from canyon incision history, southern Peru. *Geology* **35,** 523–526 (2007).
80. Sebagenzi, M. N. & Kaputo, K. Geophysical evidences of continental break up in the southeast of the Democratic Republic of Congo and Zambia (Central Africa). *Stephan Mueller Special Publication Series* **2,** 193–206 (2002).
81. Nyblade, A. A. & Pollack, H. N. A global analysis of heat flow from Precambrian terrains: Implications for the thermal structure of Archean and Proterozoic lithosphere. *J. Geophys. Res.* **98,** 12207–12218 (1993).